2015

The valine and lysine residues in the conserved FxVTxK motif are important for the function of phylogenetically distant plant cellulose synthases

Erin Slabaugh

Tess Scavuzzo-Duggan
University of Rhode Island

See next page for additional authors

Citation/Publisher Attribution
Slabaugh, E., Scavuzzo-Duggan, T., Chaves, A., Wilson, L., Wilson, C., Davis, J. K., Cosgrove, D. J., Anderson, C. T., Roberts, A. W., & Haigler, C. H. The valine and lysine residues in the conserved FxVTxK motif are important for the function of phylogenetically distant plant cellulose synthases. *Glycobiology*. Advance online publication.
Available at: http://www.dx.doi.org/10.1093/glycob/cwv118

The valine and lysine residues in the conserved FxVTxK motif are important for the function of phylogenetically distant plant cellulose synthases

This paper appeared on-line on December 9, 2015 in *Glycobiology*, doi:10.1093/glycob/cwv118

Erin Slabaugh[1], Tess Scavuzzo-Duggan[2], Arielle Chaves[2], Liza Wilson[3], Carmen Wilson[1], Jonathan K. Davis[1], Daniel J. Cosgrove[3], Charles T. Anderson[3], Alison W. Roberts[2] and Candace H. Haigler[1]

[1]Department of Crop Science and Department of Plant and Microbial Biology, North Carolina State University, Raleigh, NC 27695, USA

[2]Department of Biological Sciences, University of Rhode Island, Kingston, RI 02881 USA

[3]Department of Biology, The Pennsylvania State University, University Park, PA 16802, USA

Corresponding author: Candace H. Haigler (chhaigle@ncsu.edu, P: 919.515.5645, F: 919.515.5315)

Key words: Cellulose synthesis/gametophore formation/phenotypic complementation/root elongation/site-directed mutagenesis

Running title: The conserved FxVTxK motif is important for CESA function

Supplementary data: Figures S1-S7, Tables S1-S3

Abstract

Cellulose synthases (CESAs) synthesize the β-1,4-glucan chains that coalesce to form cellulose microfibrils in plant cell walls. In addition to a large cytosolic (catalytic) domain, CESAs have eight predicted transmembrane helices (TMHs). However, analogous to the structure of BcsA, a bacterial cellulose synthase, predicted TMH5 in CESA may instead be an interfacial helix. This would place the conserved FxVTxK motif in the plant cell cytosol where it could function as a substrate-gating loop as occurs in BcsA. To define the functional importance of the CESA region containing FxVTxK, we tested five parallel mutations in *Arabidopsis thaliana* CESA1 and *Physcomitrella patens* CESA5 in complementation assays of the relevant *cesa* mutants. In both organisms, the substitution of the valine or lysine residues in FxVTxK severely affected CESA function. In Arabidopsis roots, both changes were correlated with lower cellulose anisotropy, as revealed by Pontamine Fast Scarlet. Analysis of hypocotyl inner cell wall layers by atomic force microscopy showed that two altered versions of *Atcesa1* could rescue cell wall phenotypes observed in the mutant background line. Overall, the data show that the FxVTxK motif is functionally important in two phylogenetically distant plant CESAs. The results show that Physcomitrella provides an efficient model for assessing the effects of engineered CESA mutations affecting primary cell wall synthesis and that diverse testing systems can lead to nuanced insights into CESA structure/function relationships. Although CESA membrane topology needs to be experimentally determined, the results support the possibility that the FxVTxK region functions similarly in CESA and BcsA.

Introduction

Cellulose is an abundant biopolymer that is produced by all land plants as well as some bacteria, protists, algae and tunicates. Cellulose microfibrils, composed of β-1,4-glucan chains, are major structural elements of plant cell walls, which in turn are important renewable biomaterials. Plant cellulose synthases (CESAs), the glycosyltransferases that synthesize the β-1,4-glucan chains in cellulose, assemble in the plasma membrane to form rosette-type (six-lobed) cellulose synthesis complexes (CSCs; Kimura *et al.*1999). In seed plants, these typically contain three isoforms within a CESA protein family. For example, in *Arabidopsis thaliana* ten CESAs group into six clades with non-redundant roles in cellulose synthesis. Members of three clades (AtCESA1, 3 and 6-like) are required to synthesize cellulose within the primary walls of expanding cells. In contrast, seven CESA isoforms are found in the moss *Physcomitrella patens*, a non-vascular plant. These form two clades that are distinct from the clades formed by seed plant CESAs, indicating that the *CESA* families of mosses and seed plants diversified independently from a single common ancestral gene (Roberts and Bushoven, 2007).

Despite differences in protein sequence arising from independent diversification of Arabidopsis and Physcomitrella CESAs, both organisms have rosette-type CSCs that were presumably inherited from their common green algal ancestor (Roberts *et al.* 2012). These CSCs synthesize microfibrils, which may then form larger macrofibrils and/or interact with cell wall matrix polymers to form a composite cell wall (Haigler *et al*. 2014; Cosgrove, 2014). The properties of cellulosic biomaterials depend on several attributes of cellulose, including its quantity, degree of polymerization, microfibril width, degree of crystallinity, and capacity to interact with other polymers (Himmel *et al.* 2007; Pauly and Keegstra, 2008). Once we fully

understand how cellulose biosynthesis and microfibril formation are regulated, we can tailor the biophysical properties of cellulose in diverse ways to optimize various plant products.

Structural insights into cellulose synthases have been available since 2013, beginning with the solved atomic structure of a bacterial cellulose synthase (BcsA; Morgan *et al.* 2013) and the generation of a congruent *ab initio* computational model of the large cytosolic domain of a plant CESA (Sethaphong *et al.* 2013). Structural comparisons show that the mechanism of glucan chain polymerization has been generally conserved since bacteria and plants diverged, while differences in the structure, interactions and regulation of cellulose synthases have also evolved (Slabaugh *et al.* 2014a). For example, BcsA has eight transmembrane helices (TMHs), and CESA is predicted to have the same number (Figure 1A), but sequence alignments of the two proteins indicate that at least some of these TMHs are not homologous (Slabaugh *et al.* 2014a). In addition, the region joining putative TMH5 and TMH6 of CESA is predicted to face the apoplast, whereas the homologous region in BcsA is in the bacterial cytosol where it functions as a gating loop to control the access and interaction of the UDP-glucose substrate with the catalytic site (Morgan *et al.* 2014). Alternatively, if putative TMH5 in CESA were instead an interfacial helix (IF), analogous to IF3 in BcsA, the putative CESA 'gating loop' would face the cytosol of plant cells (Figure 1B). These uncertainties point to the need to obtain additional information about this region in CESA, which we will refer to as the TMH5-TMH6 region while acknowledging that putative TMH5 may in fact be an IF helix.

The 20 amino acids in the substrate-gating loop between IF3 and TMH7 in BcsA include the amino acid residues FAVTAK as part of an FxVTxK motif (Morgan *et al.* 2014). When the gating loop is in the "open" position, the phenylalanine and valine residues interact with a hydrophobic pocket created by IF2 and IF3, allowing substrate to access the active site. When

the gating loop is in the "inserted" position, the F, V, T and K residues participate in coordinating UDP in the active site (Morgan *et al.* 2014). Cyclic-di-GMP (c-di-GMP) acts as an allosteric regulator of the gating loop position by binding to the PilZ domain. When c-di-GMP is absent, the gating loop occludes the active site during a "resting" state for the protein. In the resting state, a conserved arginine (R580) in the PilZ domain interacts with the carbonyl group of a threonine (T511) in the gating loop (located three amino acids downstream of FAVTAK) and the side chain of a glutamate (E371) in the cytosolic domain, a residue that is conserved in prokaryotes (Morgan *et al.* 2014). In contrast, the gating loop moves into the "open" or "inserted" conformations when c-di-GMP is present and binds to the PilZ domain. This binding results in the 180° rotation of the R580 side chain, breaking its interaction with T511 and E371 (Morgan *et al.* 2014). Therefore, the BcsA gating loop plays a fundamental role in regulating the synthesis of β-1,4-glucan in *Rhodobacter sphaeroides*.

The residues at the T511 and E371 positions in BcsA are not conserved in plant CESAs, which also lack the regulatory PilZ domain. These differences are consistent with the absence of c-di-GMP in plants, and they again indicate the need for empirical analysis of the plant CESA TMH5-TMH6 region, which contains an FxVTxK motif (Figure 1C, Supplementary data, Figure S1). However, there are 5-10 additional amino acids between the helical regions in various CESAs as compared to BcsA, including 4-5 acidic residues in CESA as compared to 1-3 acidic residues in bacterial cellulose synthases (Figure 1C). The TMH5-TMH6 region affects CESA function as shown by three missense mutations: *Oscesa4*^{G858R} (*bc11*) in *Oryza sativa* (rice) and *Atcesa1*^{F954L} and *Atcesa3*^{T942I} (*ixr1-2*) in *Arabidopsis thaliana*. The *Oscesa4*^{G858R} mutation occurs at the end of predicted TMH5. This change of glycine to arginine results in a brittle culm, dwarfism, altered arabinoxylan and cellulose content, and resistance to a cellulose biosynthesis

inhibitor (2,6-dichlorobenzonitrile; Zhang *et al.* 2009). The change from phenylalanine to lysine in the FxVTxK motif of AtCESA1 (*Atcesa1*^{F954L}) impairs CESA1 function during root elongation (Slabaugh *et al.* 2014b). Changing the threonine residue to isoleucine in AtCESA3 (*Atcesa3*^{T942I}) confers resistance to a cellulose biosynthesis inhibitor (isoxaben), decreases cellulose content and crystallinity and increases CSC velocity at the plasma membrane (Scheible *et al.* 2001; Harris *et al.* 2012).

To further understand the functionality of the TMH5-TMH6 region in plant CESA, we tested additional missense mutations and deletion or mutation of the acidic motif in Arabidopsis AtCESA1 and Physcomitrella PpCESA5 (Table 1). We hypothesized that other conserved residues in this region would be required for function in phylogenetically distant CESAs and that the additional residues in CESA (as compared to BcsA), such as the longer acidic motif, would also be functionally important. The genetic complementation experiments took advantage of existing mutant *cesa* lines, which provided the background genotypes for expression of engineered CESAs followed by assessment of the extent of restoration of the wild-type phenotypes. For Arabidopsis experiments, we used the *Atcesa1*^{A549V} (*rsw1-1*) mutation in AtCESA1 as the background genotype. This mutation manifests as short swollen primary roots when grown at a restrictive temperature in association with disassembly of the CSC, which disrupts crystalline cellulose synthesis (Baskin *et al.* 1992; Arioli *et al.* 1998; Peng *et al.* 2000; Wang *et al.* 2008). Therefore, this mutant line acts as an effective protein null at the restrictive temperature. The focus on AtCESA1 for genetic complementation assays is supported by its knockout causing gametophytic lethality (Persson *et al.* 2007); apparently no other CESA can substitute for it within a functional CSC. Adapting methods of others (Chen *et al.* 2010; Fujita *et al.* 2013), we previously used the *Atcesa1*^{A549V} line to show that mutation of the phenylalanine in

the FxVTxK motif is detrimental to CESA function (Slabaugh *et al.* 2014b). For Physcomitrella experiments, we used a knockout line of PpCESA5 that was produced through homologous recombination and is impaired in the formation of leafy gametophores due to a deficiency in crystalline cellulose (Goss *et al.* 2012). We previously established the parameters for an engineered CESA complementation assay in Physcomitrella based on this knockout mutant (Scavuzzo-Duggan *et al.* 2015).

The results reported here, together with prior results on one Arabidopsis missense mutation (Slabaugh *et al.* 2014b), demonstrate that the phenylalanine, valine, and lysine residues in the FxVTxK motif are essential for normal function of AtCESA1 and PpCESA5, representing two phylogenetically distant land plant CESAs. Cell wall characteristics were analyzed on selected Arabidopsis mutants to show that mutations in AtCESA1 were sometimes associated with changes in cellulose anisotropy in roots, while other cell wall architecture phenotypes in the *Atcesa1*^{A549V} mutant line were complemented in hypocotyls. In contrast, deletion or mutation of the acidic residues had milder or no effects on the developmental phenotypes, with some differences observed between the Arabidopsis and Physcomitrella assays. Possible reasons for the differences are discussed, along with the implications for future assessments of CESA function through genetic complementation assays. The data also showed that the radial swelling and root elongation phenotypes are separable in *Atcesa1*^{A549V}, and they have implications for the possible differential effects of one inactive CESA within the CSC as compared to non-functionality of the entire CSC. In general, the results support the possibility of conserved function of the region containing the FxVTxK motif in diverse cellulose synthases over evolutionary time.

Results

Effects on Arabidopsis primary root development due to changes in the TMH5-TMH6 region of AtCESA1

As expected, root elongation was inhibited compared to the Col-0 wild type line when the *Atcesa1*^{A549V} mutant line was exposed to a restrictive temperature of 29°C (Figure 2A). Expressing wild type *CESA1* in the mutant background line under control of the native promoter as a positive control (*AtCESA1*$^{wild\ type}$) allowed roots to elongate normally at the restrictive temperature. Five mutations in *CESA1* were tested in this complementation assay. Two of these, *Atcesa1*^{V956D} and *Atcesa1*^{K959E}, were unable to rescue the short root phenotype. Three mutations [*Atcesa1*^{T952V}; deleting the acidic motif (DEDGD, *Atcesa1*$^{deleted\ acidic\ motif}$); and mutating the acidic motif to remove the acidic charge (changing DEDGD to NQNGN, *Atcesa1*$^{mutated\ acidic\ motif}$)] resulted in intermediate root length compared to the *Atcesa1*^{A549V} mutant line and the positive control.

Evidence that mutant CESAs were present when Arabidopsis roots remained short

Contrary to the variable effects on root length just described, all of the experimental lines including the positive control rescued the radial swelling of the root tip that is characteristic of the *Atcesa1*^{A549V} mutant line when exposed to a restrictive temperature (Figure 2B). We interpret this effect as supporting: (a) protein expression in each of the experimental lines; and (b) the assembly of the CSC in the five TMH5-TMH6 mutant lines (see Discussion).

Partial rescue of the root length phenotype for three mutations provides additional evidence that the mutant proteins are expressed and can function to a limited degree. For the two mutant proteins that did not rescue the root length phenotype (*Atcesa1*^{V956D} and *Atcesa1*^{K959E}) we

conducted additional experiments to support the conclusion that lack of phenotypic complementation was due to aberrant CESA1 function and not a lack of protein expression. For *Atcesa1*^{K959E}, we implemented an established strategy of expressing the mutant protein in the *Atcesa6*^{prc1} *Atcesa1*^{A549V} YFP-CESA6 background (hereafter referred to as *Atcesa1*^{A549V} YFP-CESA6) in order to monitor CSC presence and subcellular localization by laser scanning confocal microscopy (Chen *et al.* 2010; Fujita *et al.* 2013; Slabaugh *et al.* 2014b). The fluorescent tag on CESA6 marks the presence of intact heteromeric CSCs and provides an indirect confirmation of the expression of the experimental CESA1 allele. When *Atcesa1*^{A549V} YFP-CESA6 hypocotyls are grown at a permissive temperature (22°C), YFP-CESA6 can be visualized near the plasma membrane as small fluorescent puncta (Supplementary data, Figure S2B) because the A549V substitution does not cause CSC disassembly at the permissive temperature. In contrast, when the hypocotyls are shifted to a restrictive temperature (27 or 29°C), YFP-CESA6 fluorescence becomes depleted near the plasma membrane due to CSC disassembly (Supplementary data, Figure S2E and S3B; Arioli *et al.* 1998; Wang *et al.* 2008; Chen *et al.* 2010; Fujita *et al.* 2013). The positive control line, *Atcesa1*^{A549V} YFP-CESA6 *AtCESA1*$^{wild\ type}$, showed YFP fluorescence near the plasma membrane at all three growth temperatures (Supplementary data, Figure S2A, D and S3A; Chen *et al.* 2010; Fujita *et al.* 2013). Similarly, the *Atcesa1*^{A549V} YFP-CESA6 *Atcesa1*^{K959E} hypocotyls also showed small fluorescent puncta at the plasma membrane at both permissive (22°C) and restrictive (29°C) growth temperatures (Supplementary data, Figure S2C, F, respectively). These observations were confirmed by determining the density of the fluorescent plasma membrane particles (Supplementary data, Figure S2G), and the combined data are consistent with *in vivo* expression of AtCESA1^{K959E}.

This approach was not effective for the *Atcesa1*^{V956D} line due to the inability to identify any *Atcesa1*^{A549V} YFP-CESA6 *Atcesa1*^{V956D} line with sufficiently high YFP expression, despite analyzing many individual transformant lines. Alternatively, we used allele-specific quantitative real-time PCR (qRT-PCR) to specifically amplify sequences containing the codon for aspartic acid in the mutant allele and not the valine in the wild type allele. The expression of the D956 mutant allele was 7 to 14 fold higher in two independent *Atcesa1*^{V956D} lines as compared to Col-0 or the *Atcesa1*^{A549V} mutant lines (Supplementary data, Figure S4A). We further confirmed that the total amount of *CESA1* mRNA was in the normal range for all the lines tested by using common primers that amplified all three *AtCESA1* alleles (wild type, *Atcesa1*^{V549} and *Atcesa1*^{D956}; Supplementary data, Figure S4B). Overall, the data are consistent with the rescue of the root swelling phenotype and support the likelihood that the short roots observed at the restrictive temperature in the *Atcesa1*^{V956D} seedlings arise from the presence of an AtCESA1^{V956D} protein with compromised functionality.

Cellulose microfibril anisotropy and cell wall architecture in Atcesa1 mutants

We used laser scanning confocal microscopy to analyze the fluorescence of cellulose-binding Pontamine Fast Scarlet (S4B; Anderson *et al.* 2010; Miart *et al.* 2014) and the FibrilTool plug-in for ImageJ (Boudaoud *et al.* 2014) to analyze cellulose microfibril alignment in the hydrated roots of the Arabidopsis mutant lines (Figure 3). Seedlings were grown for five days at a lower restrictive temperature (27°C instead of 29°C) in order to support germination and sufficient seedling growth to allow these analyses to be conducted. Even at high magnifications, the microfibril patterns are not discernable by eye in the images, which are displayed in Supplementary data Figure S5. The quantitative output of the FibrilTool is shown in Figure 3:

the anisotropy values are unitless, with a score of 0 representing no order and a score of 1 representing perfect order (Boudaoud *et al.* 2014). Consistent with their failure to rescue the short root phenotype (Figure 2A), the roots of the *Atcesa1*^{V956D} and *Atcesa1*^{K959E} lines showed lower cellulose anisotropy values that were similar to the *Atcesa1*^{A549V} line (Figure 3). In contrast, the three lines that showed partial rescue of the root length phenotype (*Atcesa1*^{T952V}, *Atcesa1*$^{mutated\ acidic\ motif}$ and *Atcesa1*$^{deleted\ acidic\ motif}$) did not show any significant change in anisotropy as compared to Col-0 and the *AtCESA1*$^{wild\ type}$ positive control line (Figure 3). Given the lower restrictive temperature used in this experiment, we confirmed that the root length phenotypes were generally similar in the TMH5-TMH6 mutants at 27°C (Figure 4A) as compared to 29°C (Figure 2A). We also confirmed that the CSCs remained depleted from the plasma membrane of hypocotyls when *Atcesa1*^{A549V} YFP-CESA6 was exposed to 27°C (Supplementary data, Figure S3). Because the laser scanning microscopy used to detect CSCs and atomic force microscopy (see below) were conducted on hypocotyls grown in the dark at 27°C, the hypocotyl length was also determined in all of the genotypes (Figure 4B). The *Atcesa1*^{V956D} and *Atcesa1*^{K959E} mutations caused proportionally less severe effects on hypocotyl elongation as compared to root elongation (compare Figure 4A, B; see Discussion).

Atomic force microscopy (AFM) was used to analyze the architecture of the innermost layer of hydrated hypocotyl cell walls at higher resolution. The hypocotyls were assayed because this organ is more amenable to AFM analysis with consistent results within a genotype (Lei *et al*. 2014). The lines analyzed included Col-0, *Atcesa1*^{A549V}, and two TMH5-TMH6 mutants, *Atcesa1*^{T952V} and *Atcesa1*^{V956D}, both of which had reduced hypocotyl elongation when grown for 5 days at 27°C (Figure 4B). Only the *Atcesa1*^{A549V} mutant line showed consistently disordered inner cell wall architecture (Figure 5A-D), and it was also the only line that had thicker cell wall

fibrils compared to the Col-0, *Atcesa1*^{T952V} and *Atcesa1*^{V956D} lines (Figure 5E). The *Atcesa1*^{A549V} cell walls also had a wider distribution of fibril widths due to the presence of thicker fibrils as compared to the other lines analyzed. For all lines analyzed, most of the fibril widths are substantially larger than the estimated 3 nm maximum diameter of a single cellulose microfibril emanating from one CSC (Fernandes *et al.* 2011; Zhang *et al.* 2014), implying that the fibrils represent higher order assembly in the cell wall due to cellulose-cellulose and/or cellulose-matrix interactions (Zhang *et al*. 2015). Cumulatively, the results show that two altered *v*ersions of *Atcesa1* could rescue severe cell wall defects in the *Atcesa1*^{A549V} line grown at restrictive temperature, although hypocotyl elongation occurred to an intermediate extent compared to the control and *Atcesa1*^{A549V} lines (Figure 4B).

Effects on Physcomitrella gametophore formation as a result of changes in the TMH5-TMH6 region of PpCESA5

A parallel set of changes in the TMH5-TMH6 region of PpCESA5 was tested by complementation of the *Ppcesa5* knockout line with abnormal gametophore formation (Figure 6; Goss *et al.* 2012). In addition, the equivalent of the F954L mutation for Arabidopsis CESA1 (Slabaugh *et al.* 2014b) was tested (Supplementary data, Figure S6). (Note that the numbering of PpCESAs is arbitrary because the CESA gene family diversified independently within the seed plant and moss lineages, resulting in no CESA orthologs between Arabidopsis and Physcomitrella.) For these assays, samples of protoplasts prepared from the knockout line were transformed with mutant PpCESA5 constructs in parallel with the positive control (*PpCESA5*$^{wild\ type}$) and the empty vector as a negative control. The resulting stable transgenic lines (10-65 per genotype) were analyzed for gametophore formation. Generally, complementation of the

Ppcesa5 knockout line resulted in approximately 60-80% of colonies that produced normal gametophores.

Similar to the compromised function of AtCESA1 with the F954L mutation (Slabaugh *et al.* 2014b), the F956L mutation in *PpCESA5* (*Ppcesa5*^{F956L}) failed to support normal gametophore formation (Supplementary data, Figure S6). Reflecting substitution of valine and lysine in the FxVTxK motif, fewer of the *Ppcesa5*^{V958D} and *Ppcesa5*^{K961E} lines produced gametophores compared to the positive controls (Figure 6). Western blot analysis confirmed that the colonies that did not produce gametophores were expressing *Ppcesa5*^{F954L}, *Ppcesa5*^{V958D} or *Ppcesa5*^{K961E} (Supplementary data, Figure S7). The other changes tested in Physcomitrella [*Ppcesa5*^{T954V}, deleting the acidic motif and mutating the acidic motif (changing DDED to NNQN)], did not affect the number of lines that produced gametophores (Figure 6).

Discussion

These results together with others (Slabaugh *et al.* 2014b) demonstrate the importance of the F, V, and K residues of the widely conserved FxVTxK motif for the function of CESAs involved in primary wall synthesis in phylogenetically distant Arabidopsis and Physcomitrella. When phenylalanine, valine, or lysine was substituted with another amino acid with different properties in AtCESA1 or PpCESA5 (see Table 1), the altered *cesa* genes failed to complement the relevant mutants: Arabidopsis roots remained short or fewer gametophores formed in Physcomitrella. Impairment of CESA function by a single alternate amino acid was supported by evidence that the altered proteins accumulated in the experimental lines. The conserved threonine in the same motif has been shown to modulate protein activity in AtCESA3, another CESA involved in seed plant primary wall formation (Scheible *et al.* 2001; Harris *et al.* 2012).

In bacterial BscA, the F, V, T, and K residues in the FxVTxK motif bind to UDP as the UDP-glucose substrate for cellulose polymerization is inserted into the active site (Morgan *et al.* 2014). Such a role is not yet established for plant CESAs. However, if this motif were on the outside of the plasma membrane, as suggested by predictions of CESA TMH topology, it would not be able to participate in substrate gating. Given the experimental evidence that each of the F, V, T and K residues continues to be important for plant CESA function, it is more likely that FxVTxK exists in the cytosol of plant cells where it could function in substrate gating as in BcsA. This conformation would be generated if CESA TMH5 were an IF helix instead of a TMH. A solved atomic structure for plant CESA is needed to resolve its topology definitively. In the meantime, biochemical experiments are in progress to test plant CESA topology empirically.

All of the mutations tested in Arabidopsis rescued the radial swelling phenotype of *Atcesa1*^{A549V} regardless of the ability of the mutant proteins to rescue the primary root length or cellulose anisotropy phenotypes. Only the *Atcesa1*^{A549V} mutant line showed persistent root swelling at a restrictive temperature in the complementation experiments, just as it was the only line tested that had a disordered inner cell wall layer and wider cell wall fibrils in AFM analysis of hypocotyls grown at restrictive temperature. These severe cell wall defects in the *Atcesa1*^{A549V} line at the 27°C restrictive temperature are consistent with the disassembly of the CSC and disruption of crystalline cellulose synthesis observed at higher restrictive temperatures (Baskin *et al.* 1992; Arioli *et al.* 1998; Peng *et al.* 2000; Wang *et al.* 2008). Our data suggest that even a functionally impaired AtCESA1 protein could substitute within the CSC and restore normal root width, as long as the experimental amino acid change allowed the CSC to persist at the plasma membrane at restrictive temperature. The data further imply that two functional CESA isomers (e.g. AtCESA3 and AtCESA6 or AtCESA6-like) are able to support the synthesis of cellulose

sufficiently to prevent root swelling. In contrast, normal root and hypocotyl elongation did not occur when the function of the FxVTxK motif in AtCESA1 was compromised, indicating that potential factors such as increased demands on the cellulose microfibril system or increased activity within cell wall integrity sensing mechanisms come into play during these elongation processes as compared to constraining the diameter of the root tip. The persistent short roots at restrictive temperature in the *Atcesa1*^{V956D} and *Atcesa1*^{K959E} lines, as well as the *Atcesa1*^{A549V} mutant line, correlated with their lower cellulose anisotropy as revealed by S4B staining in comparison to Col-0 and other mutant lines. This result is consistent with the well known role of anisotropic cellulose in helping to regulate the expansion of plant cells and organs (Baskin, 2005; Szymanski and Cosgrove, 2009). Presently, we do not know how the mutation of single residues in the TMH5-TMH6 region of AtCESA1 could affect cellulose microfibril organization in the primary cell wall. This effect could arise through changes in the rate of β-1,4-glucan polymerization, cell expansion, or cell wall integrity sensing (Liu *et al*. 2015).

Comparison and contrast of phenotypic effects of Atcesa1 mutations

Measuring primary root lengths of seedlings grown for five days at permissive temperature followed by two days at restrictive temperature is commonly used in experiments involving the *Atcesa1*^{A549V} mutant line (Baskin *et al.* 1992; Arioli *et al*. 1998; Fujita *et al*. 2013), and this temperature regime was also used in our experiments (Figure 2). However, it was difficult to analyze the cell wall characteristics of such plants due to heterogeneous walls formed at different temperatures. Initial efforts to grow *Atcesa1*^{A549V} seedlings at constant 29°C failed due to very low rates of germination and subsequent growth. Sufficient and more homogeneous cell walls were generated for further analysis by use of 27°C as a lower but still restrictive

temperature, as demonstrated by clearing of CSCs from the plasma membrane and inhibition of root and hypocotyl elongation in the *Atcesa1*^{A549V} line (Figure 4, Supplementary data, Figure S3).

During the phenotypic analysis, we observed similar trends between temperature regimes along with differences between organ types when comparing mutant and control lines after five days of growth at 27°C. Under this growth regime, the elongation of light-grown primary roots remained greatly inhibited in the *Atcesa1*^{K959E} and *Atcesa1*^{V956D} seedlings (about 28% of Col-0 on average), similar to the *Atcesa1*^{A549V} mutant line except for slightly greater elongation of the *Atcesa1*^{K959E} roots (Figure 4A). In contrast, the elongation of the dark-grown hypocotyls in the *Atcesa1*^{K959E} and the *Atcesa1*^{V956D} seedlings was much greater than in the *Atcesa1*^{A549V} mutant line and closer to the control values (about 65% of Col-0 on average). This difference between degree of growth inhibition in roots and hypocotyls did not occur in the context of overall milder phenotypes at restrictive temperature in *Atcesa1*^{T952V} or when the *AtCESA1* acidic motif was mutated or deleted: after complementation with each of these variant genes, both roots and hypocotyls elongated to about 75% of Col-0 values on average. For the *Atcesa1*^{V956D} line that was analyzed by both S4B staining and AFM after growth at restrictive temperature: (a) the greatly hindered root elongation (Figure 4A) is consistent with low cellulose anisotropy (Figure 3) like the *Atcesa1*^{A549V} mutant line (Figure 3); and (b) the less hindered hypocotyl elongation (Figure 4B) is consistent with the relatively normal inner cell wall layer (Figure 5D, E) in contrast to the altered cell wall architecture and fibril width phenotypes in the short hypocotyls (Figure 4B) of the *Atcesa1*^{A549V} mutant line (Figure 5B, E). The differences observed between the extent of elongation of light-grown roots and dark-grown hypocotyls of the *Atcesa1*^{V956D} and *Atcesa1*^{K959E} mutants may relate to light-mediated regulation of cellulose synthesis (Desnos *et al*.

1996; Bischoff et al. 2011), which may have stronger impacts when cellulose synthesis is severely impaired through particular changes in the CESA sequence.

Assessment of Physcomitrella as a rapid screening system for probing CESA structure/function relationships

Arabidopsis and Physcomitrella sometimes responded differently to homologous changes in their CESAs. For example, *Atcesa1* carrying mutations in the F, V or K residues did not rescue root elongation at restrictive temperature, whereas various degrees of partial rescue of the gametophore phenotype occurred upon making the parallel changes in Physcomitrella. Substitution of the K residue had the strongest negative impact in Physcomitrella, whereas substitution of F956L still allowed approximately two thirds of the colonies to produce gametophores compared to $PpCESA5^{wild\ type}$ in moss (Figure 6, Supplementary data, Figure S6). Other differences between organisms were observed upon substituting the plant-conserved threonine two residues upstream of FxVTxK, mutating the acidic motif to contain neutral amino acids, or deleting the acidic motif. These changes did not affect gametophore formation in Physcomitrella, whereas root growth at restrictive temperature remained partly hindered in Arabidopsis. Possibly, the residues surrounding FxVTxK have acquired functions during land plant evolution, regulating plant CESA function through fine control mechanisms that remain to be determined.

Overall, the results show that the PpCESA5 complementation assay in Physcomitrella is useful for identifying residue and motif changes that are likely to have substantial impacts on AtCESA1 function and organ elongation in seed plants. Testing mutations in PpCESA5 can be completed as rapidly as seven weeks with several tests run in parallel (Scavuzzo-Duggan *et al.*

2015), whereas testing multiple mutations by Arabidopsis plant transformation can take up to six months. Based on these initial trials of the two complementation systems run in parallel, 40% of the moss assays on PpCESA5 would produce changes in gametophore number that would be paralleled by changes in organ elongation in Arabidopsis. Our previous work showed that the change of a widely conserved arginine to lysine (a R453K mutation in PpCESA5) only partially rescued gametophore formation, whereas no gametophores were formed in the R453D line (Scavuzzo-Duggan *et al*. 2015). The R453K mutation is analogous to the relatively mild Arabidopsis *fra6* mutation in AtCESA8 (Zhong *et al*. 2003). Therefore, the moss complementation system can also be used in the future to test the effects of different amino acid substitutions at one location.

The different developmental contexts of the assays in each organism may have impacted the currently reported comparisons of the effects of parallel changes in phylogenetically distant CESAs. AtCESA1 is required for both gametogenesis and embryo viability through participating in cytokinesis and cell plate formation as well as for formation of the typical primary walls of expanding cells (Arioli *et al.* 1998; Gillmor *et al.* 2002; Beeckman *et al.* 2002; Persson *et al.* 2007; Miart *et al.* 2013). In contrast, PpCESA5 functions specifically in formation of reproductive gametophores, and it is not required during protonemal growth (Goss *et al.* 2012). The development of thin planar gametophores may be less sensitive to alterations in microfibril structure compared to root elongation in Arabidopsis. Alternatively, particular CESA isoforms in different organisms may have specific functions that will only be uncovered through future experiments. Presently, we have only limited and indirect data about the functional differences between CESA isoforms in any plant. For example, the rate of CSC movement in the plasma membrane was slower in dark-grown hypocotyls when AtCESA5, an isoform in the same clade

as AtCESA6, became integrated into the CSC of an AtCESA6 knock-out line (Bischoff *et al*. 2011). Conversely, when a 'secondary wall' CESA was used to complement a mutation in a 'primary wall' CESA, the rate of CSC movement became faster than in the control line (Carroll *et al*. 2012). Understanding the mechanistic implications of the different CESA clades, both between Phycomitrella and the seed plants and within the seed plants, remains an important avenue for future research on cellulose synthesis. Parallel testing of the effects of structural changes in multiple CESA isoforms as we have demonstrated here will accelerate the pace of discovery in this area and ultimately lead to additional useful outcomes of CESA structural engineering.

Materials and methods

Chemicals and kits

All chemicals and kits were acquired from Sigma-Aldrich (St. Louis, MO) unless otherwise noted.

Statistical Analysis

Unless otherwise noted, ANOVA along with Tukey-Kramer post hoc analysis was used to test statistical differences and establish groups of means.

Production and growth of transgenic Arabidopsis lines

All of the TMH5-TMH6 mutant *cesa* genes used in this study were expressed in either the *Atcesa1*^{A549V} or *Atcesa6*^{prc1} *Atcesa1*^{A549V} YFP-CESA6 background, using previously described methods (Slabaugh *et al.* 2014b). These lines share the temperature sensitive *Atcesa1*^{A549V}

mutation, and the latter line integrates a YFP label on CESA6 within the heteromeric CSC. The mutation lines expressed in the *Atcesa1*^{A549V} background are described in the text by the location of the experimental amino acid substitution or nature of a motif change for clarity.

The native *AtCESA1* (At4g32410) promoter sequence, including the 5'UTR and 1 kb sequence upstream of the 5'UTR, was used to drive the expression of AtCESA1 mutant and wild type sequences. Site-directed mutagenesis was carried out via overlap PCR (Ho *et al.* 1989) using mutagenesis primers (Supplementary data, Table S3). Transformants resistant to the herbicide glufosinate ammonium were identified by spraying two-week-old seedlings sown on soil with a mixture of 0.056 mg/L glufosinate ammonium and 0.04% (v/v) Silwet L-77 surfactant (Lehle Seeds, Round Rock, TX) three times a week until selection was complete. Survivors were confirmed as positive transformants by genotyping. Subsequent generations were selected on ½ strength Murashige and Skoog (MS) plates that contained 1% (w/v) sucrose, 5 mg/mL glufosinate ammonium and 0.4% (w/v) Phytagel under constant light for two weeks before transplanting seedlings to soil for seed propagation.

Assessing root and hypocotyl phenotypes in transgenic Arabidopsis lines

All phenotypes were characterized in at least two independent homozygous transgenic lines (at T2 or subsequent generations). Details of experimental temperature regimes are specified where appropriate in the text. Primary root length at 29°C was analyzed in seedlings expressing AtCESA1 wild type and mutant constructs in the *Atcesa1*^{A549V} and *Atcesa6*^{prc1} *Atcesa1*^{A549V} *YFP-CESA6* backgrounds. Radial swelling, hypocotyl length and root length at 27°C was only analyzed in the *Atcesa1*^{A549V} background, except for in the *Atcesa1*$^{mutated\ acidic\ motif}$ mutant, which was analyzed in the *Atcesa6*^{prc1} *Atcesa1*^{A549V} *YFP-CESA6* background. Phenotypic data were

consistent between all independent transgenic lines tested for each mutant. Representative data from one line were used to display phenotypic data graphically. A complete list of root length data for each independent mutant line analyzed when grown for 5 d at 22°C and 2 d at 29°C can be found in Supplementary material Table S2.

For assessing root phenotypes, seeds from *Atcesa1* mutant expression lines, along with seeds from wild type (Col-0), *Atcesa1*^{A549V} and *Atcesa6*^{prc1} *Atcesa1*^{A549V} *YFP-CESA6* as controls, were grown vertically on ½ strength MS plates with 1% (w/v) sucrose and 0.4% (w/v) Phytagel. Seedlings were grown under continuous light (100 μmol/m^2/sec) to measure root lengths, or in the dark by wrapping plates in aluminum foil to measure hypocotyl lengths. All plates were grown at 50% relative humidity. For root and hypocotyl length measurements, seedlings on plates were photographed and then analyzed using ImageJ (http://rsbweb.nih.gov/ij/). At least three independent experimental replicates were performed in all cases, and n values for measurements are indicated in each figure legend. For radial swelling analysis, seedlings were preserved in Histochoice MB fixative (Electron Microscopy Sciences, Hatfield, PA) and digital images of the root tips were collected using a light microscope. The seedlings were mounted horizontally on a slide with scotch tape placed on one side nearest to the root tip to protect it from being distorted by the cover slip. Diameter measurements were made in ImageJ at the widest part of the root tip, within 1-2 mm from the point where the root initials and root cap separate: this location is where the swelling of the root tip is the most severe (Baskin *et al.* 1992; Williamson *et al.* 2001).

Quantitative RT-PCR on Arabidopsis seedlings

Seedlings were grown as described above for root phenotyping. Three seedlings were pooled per sample, tissue was flash frozen in liquid nitrogen and RNA was extracted using the Spectrum Plant Total RNA kit. cDNA synthesis was carried out using the TaqMan kit (Applied Biosystems, Grand Island, NY) with random hexamers and 600 ng of RNA per reaction. DNase digestion was performed with the DNaseI Digestion kit. Quantitative RT-PCR was carried out using SYBR Green and an ABI 7300 Real-Time PCR System (Applied Biosystems, Grand Island, NY) with a 30 μL reaction volume and 20 ng of RNA per sample. UBQ10 (AT4G05320) was used as an internal control (Czechowski *et al.* 2005). Three separate experiments were preformed, each containing two biological and three technical replicates. Fold change was measured relative to Col-0. For a list of primers, see Supplementary data, Table S3.

Laser scanning confocal microscopy

All analyses were performed with a spinning disk confocal microscope (Observer SD, Zeiss, Thornwood, NY) equipped with a 100X 1.40 NA oil-immersion objective and an electron multiplying gain camera (QuantEM 512SC, Photometrics, Tucson, AZ).

For subcellular localization of YFP-CESA6 in Arabidopsis hypocotyls, seeds were sterilized for 20 minutes in 30% bleach + 0.1% SDS in water, then were washed four times with sterile water and suspended in sterile 0.15% agar-agar (Research Organics, Cleveland, OH) at 4°C for 3-10 days. Seedlings expressing YFP-CESA6 were grown in the dark on ½ strength MS plates without sucrose for either three days at 22°C (permissive temperature) or for two days at 22°C, then shifted to 27°C or 29°C for one day (restrictive temperatures). For all genotypes, YFP fluorescence was detected in hypocotyl cells just below the apical hook using a 100 mW 488 nm excitation laser at 100% power and a 525/50 nm emission filter. All images were collected at the

same exposure time (400 ms, EM gain=1000, readout gain=2). Z-series were captured using a slice interval of 0.2 μm. Substacks were generated of each z-series that were inclusive of the plane of the plasma membrane for YFP-CESA6 particle density analysis and particle density was quantified computationally using the Spot Detection function of Imaris (Bitplane, Zurich, Switzerland) (Chen *et al.* 2010) with a spot size of 0.25 μm.

For analysis of cellulose anisotropy after S4B staining of Arabidopsis roots, seeds were surface sterilized as described above and sown on plates containing ½ strength MS salts, 0.6 g/L MES (2-ethanesulfonic acid), 0.8% (w/v) agar-agar (Research Organics, Cleveland, OH), 1% (w/v) sucrose, pH 5.6 and incubated in a growth chamber (Percival CU-36L5, Perry, IA) under constant light at 27°C for 5 days. Seedlings were stained with 0.01% (w/v) Pontamine Fast Scarlet 4B (S4B; aka Direct Red 23; Anderson *et al.* 2010) in liquid MS medium for 30 minutes, and the walls of root elongation zone epidermal cells were imaged using a 561 nm excitation laser and a 617/73 emission filter. Identical settings were used to capture all images. Image stacks were projected and contrast enhanced in ImageJ, then the anisotropy of microfilbrils was measured in individual root cells using the FibrilTool plug-in (Boudaoud *et al.* 2014). For each genotype at least 39 cells were measured across three experimental trials in three individual seedlings per trial.

Atomic force microscopy of inner cell walls of Arabidopsis hypocotyls

Sterilized seeds were stored in 100 μL distilled water in the dark at 4°C for 24-72 hours before plating (50 seeds per mutant) on ½ strength MS plates with 0.6 g/L MES (2-ethanesulfonic acid) and 0.8% (w/v) agar-agar (EMD Science, Billerica, MA) at pH 5.6. Samples were grown vertically in the dark for five days at 27°C.

Between 30 and 50 dark-grown whole hypocotyls for each mutant and Col-0 were excised using a razor blade after removing the root and cotyledons. Preparation of cell wall fragments was similar to published methods (Lei *et al.* 2014). Briefly, samples were ground in liquid nitrogen using a plastic pestle and bench press drill (Model #137.219090; Sears, Hoffmann Estates, IL) modified to run at 620 rpm, and thawed in 500 μL of 20 mM HEPES [N-(2-hydroxyethyl) piperazine-N′-(2-ethanesulfonic acid], pH 7.5, plus 0.1% (v/v) Tween 20 detergent. The cell wall fragments were washed twice by repeated centrifugation (3000 x g, 2 sec), removal of the supernatant, and resuspension in fresh buffer with vortexing. Finally, samples were resuspended in 100 μL buffer and agitated (rocking, 30 min) prior to centrifugation and resuspension in 50 μL of 20 mM HEPES, pH 7.5, with no detergent. A drop of sample (5 μL) was partially, but not completely, dried on a slide, which caused the cuticle side of the hypocotyl cell wall fragments to adhere. Following rinsing in buffer to remove unbound fragments, samples were observed in the hydrated state with an AFM instrument (Dimension Icon system with a NanoScope V controller; Bruker Corporation, Santa Barbara, CA)

AFM data were acquired using the tapping PeakForce QNM program under fluid conditions with a ScanAsyst Fluid+ tip with a nominal spring constant of 0.7 N/m, as reported by the manufacturer. The tapping PeakForce QNM scanning parameters were controlled by the system software to achieve the best topography resolution, except for the scan rate which was set at a constant tip velocity of 1.7 μm/s. The optical imaging mode was used to select cells with entire borders for image capture at 1 x 1 μm with 384 x 384 pixels. Images were acquired from 6 cells (for Col-0, with the most uniform cell wall architecture) or 14 to 19 cells (for the experimental lines) within individual cell wall fragments. Original AFM height images were plane fitted and flattened using Nanoscope Analysis 1.5v software (Bruker Corporation,

Billerica, MA). The fibril width measurements (200 per sample) were acquired from at least 4 clear and representative images per genotype using the same software. For each image, three 350 nm transect lines were drawn at random locations, and the baseline was determined by hand prior to measuring the widths of all peaks with defined edges as described in Zhang *et al*. 2015. The Fluid+ tip radius was determined to be approximately 1.8 nm in previous work (Zhang *et al.* 2014), leading to the subtraction of 3.6 nm from the raw measurements.

Physcomitrella assays

Detailed methods related to the moss assays have been published previously (Scavuzzo-Duggan *et al.* 2015). For vector construction, entry vectors carrying *PpCESA5* coding sequences with point or deletion mutations were constructed by PCR fusion and Gateway cloning (Atanassov *et al.* 2009) using primers listed in Supplementary data, Table S3. The mutated coding sequences in pDONR P5-P2 were transferred along with a triple HA tag in pDONR P1-P5r to the pTHAct1-Gate destination vector using LR Clonase II Plus (Life Technologies, Grand Island, NY, USA). pTHAct1-Gate is targeted to the intergenic 108 locus, confers hygromycin resistance, and drives constitutive expression of the transgene via the rice *Act1* promoter (Perroud and Quatrano, 2006).

For each complementation experiment, samples of protoplasts prepared from a *PpCESA5* knockout line *ppcesa*5KO-2 (Goss *et al.* 2012) were transformed with one of 3-4 test vectors carrying different mutated 3XHA-tagged *PpCESA5* coding sequences, a positive control wild type 3XHA-*PpCESA5* expression vector or a negative control empty vector. Regenerated protoplasts were selected through two rounds of hygromycin treatment and stable transformants were arrayed on solid medium and incubated. Complementation was scored by counting the

number of stably transformed colonies that produced gametophores. Data were collected from transformations that produced 10 or more stable transformants. For each test vector, the numbers of stably transformed colonies with and without gametophores were compared to the positive and negative controls using pooled counts from two independent experiments and a two-tailed Fisher's exact test of independence (Sokal and Rohlf 1981).

For protein expression analysis, microsomal proteins were extracted from stably transformed colonies, separated by SDS-PAGE and transferred to membranes. The membranes were stained for total proteins with Ponceau S and probed with anti-HA to detect transgenic protein expression.

Supplementary data

Supplementary data for this article are available online at http://glycob.oxfordjournals.org/.

Funding

This work was supported as part of The Center for LignoCellulose Structure and Formation, an Energy Frontier Research Center funded by the U.S. Department of Energy, Office of Science, Basic Energy Sciences under Award # DE-SC0001090. Vector sequencing for the Physcomitrella experiments was conducted in the Rhode Island Genomics and Sequencing Center, which is supported in part by the National Science Foundation under EPSCoR Grants Nos. 0554548 & EPS-1004057.

Acknowledgements

We would also like to thank Dr. Chris Somerville for providing the seeds of *Atcesa6*^{prc1} *Atcesa1*^{rsw1} YFP-CESA6 and *Atcesa6*^{prc1} *Atcesa1*^{rsw1} YFP-CESA6 AtCESA1 and Dr. Pierre-Francois Perroud for providing the pTHAct1-Gate vector. We also thank Dr. Tian Zhang for helpful discussions on AFM fiber width measurements and protocols.

Abbreviations

AFM atomic force microscopy

CESA cellulose synthase

c-di-GMP cyclic di-GMP or cyclic diguanylate

CSC cellulose synthesis complex

IF interfacial helix

S4B Pontamine Fast Scarlet

TMH transmembrane helix

YFP yellow fluorescent protein

References

Anderson, C.T., Carroll, A., Akhmetova, L. and Somerville, C. 2010. Real-time imaging of cellulose reorientation during cell wall expansion in Arabidopsis roots. *Plant Physiol.* 152:787–796.

Arioli, T., Peng, L., Betzner, A.S., Burn, J., Wittke, W., Herth, W., Camilleri, C., Hofte, H., Plazinski, J., Birch, R., Cork. A., Glover, J., Redmond, J., Williamson, R.E. 1998. Molecular analysis of cellulose biosynthesis in Arabidopsis. *Science.* 279:717-720.

Atanassov, I.I., Pittman, J.K. and Turner, S.R. 2009. Elucidating the mechanisms of assembly and subunit interaction of the cellulose synthase complex of Arabidopsis secondary cell walls. *J Biol Chem.* 284:3833–3841.

Baskin, T.I. 2005. Anisotropic expansion of the plant cell wall. *Annu Rev Cell Dev Biol.* 21:203–222.

Baskin, T.I., Betzner, a S., Hoggart, R., Cork, a and Williamson, R.E. 1992. Root morphology mutants in Arabidopsis thaliana. *Funct Plant Biol.* 19:427–437.

Beeckman, T., Przemeck, G.K.H., Stamatiou, G., Lau, R., Terryn, N., Rycke, R. De, Inze, D. and Berleth, T. 2002. Genetic complexity of cellulose synthase A gene function in Arabidopsis embryogenesis. *Plant Physiol.* 130:1883–1893.

Bischoff, V., Desprez, T., Mouille, G., Vernhettes, S., Gonneau, M. and Hofte, H. 2011. Phytochrome regulation of cellulose synthesis in Arabidopsis. *Curr Biol.* 21:1822-1827.

Boudaoud, A., Burian, A., Borowska-Wykręt, D., Uyttewaal, M., Wrzalik, R., Kwiatkowska, D. and Hamant, O. 2014. FibrilTool, an ImageJ plug-in to quantify fibrillar structures in raw microscopy images. *Nat Protoc.* 9:457–463.

Carroll, A., Mansoori, N., Shundai, L., Lei, L., Vernhettes, S., Visser, R.G.F., Somerville, C., Gu, Y. and Trindade, L.M. 2012. Complexes with mixed primary and secondary cellulose synthases are functional in Arabidopsis plants. *Plant Physiol.* 160:726-737

Chen, S., Ehrhardt, D.W. and Somerville, C.R. 2010. Mutations of cellulose synthase (CESA1) phosphorylation sites modulate anisotropic cell expansion and bidirectional mobility of cellulose synthase. *Proc Natl Acad Sci USA.* 107:17188–17193.

Cosgrove, D.J. 2014. Re-constructing our models of cellulose and primary cell wall assembly. *Curr Opin Plant Biol.* 22:122-131.

Czechowski, T., Stitt, M., Altmann, T. and Udvardi, M.K. 2005. Genome-wide identification and testing of superior reference genes for transcript normalization in Arabidopsis. *Genome Anal.* 139:5–17.

Desnos, T., Orbovic, V., Bellini, C., Kronenberger, J., Caboche, M., Traas, J. and Hofte, H. 1996. Procuste1 mutants identify two distinct genetic pathways controlling hypocotyl cell elongation, respectively in dark- and light-grown Arabidopsis seedlings. *Development* 122: 683-693.

Fernandes, A.N., Thomas, L.H., Altaner, C.M., Callow, P., Forsyth, V.T., Apperley, D.C., Kennedy, C.J., Jarvis, M.C. 2011. Nanostructure of cellulose microfibrils in spruce wood. *Proc Natl Acad Sci USA.* 108:E1195-E1203.

Fujita, M., Himmelspach, R., Ward, J., Whittington, A., Hasenbein, N., Liu, C., Truong, T.T., Galway, M.E., Mansfield, S.D., Hocart, C.H. and Wasteneys, G.O. 2013. The anisotropy1 D604N mutation in the Arabidopsis cellulose synthase1 catalytic domain reduces cell wall crystallinity and the velocity of cellulose synthase complexes. *Plant Physiol.* 162:74–85.

Gillmor, C.S., Poindexter, P., Lorieau, J., Palcic, M.M. and Somerville, C. 2002. Alpha-glucosidase I is required for cellulose biosynthesis and morphogenesis in Arabidopsis. *J Cell Biol.* 156:1003–1013.

Goss, C. a, Brockmann, D.J., Bushoven, J.T. and Roberts, A.W. 2012. A CELLULOSE SYNTHASE (CESA) gene essential for gametophore morphogenesis in the moss Physcomitrella patens. *Planta.* 235:1355–1367.

Haigler, C.H., Grimson, M.J., Gervais, J., Moigne, N. Le, Höfte, H., Monasse, B. and Navard, P. 2014. Molecular modeling and imaging of initial stages of cellulose fibril assembly: Evidence for a disordered intermediate stage. *PLoS One.* 9:1–10.

Harris, D.M., Corbin, K., Wang, T., Gutierrez, R., Bertolo, A.L., Petti, C., Smilgies, D., Estavez, J.M., Bonetta, D., Urbanowicz, B.R., Ehrhardt, D.W., Sommerville, C.R., Rose, J.K., Hong, M. and DeBolt, S. 2012. Cellulose microfibril crystallinity is reduced by mutating C-terminal transmembrane region residues CESA1^{A903V} and CESA3^{T942I} of cellulose synthase. *Proc Natl Acad Sci USA.* 109:4098–4103.

Himmel, M.E., Ding, S.-Y., Johnson, D.K., Adney, W.S., Nimlos, M.R., Brady, J.W. and Foust, T.D. 2007. Biomass recalcitrance: engineering plants and enzymes for biofuels production. *Science.* 315:804–807.

Ho, S.N., Hunt, H.D., Horton, R.M., Pullen, J.K. and Pease, L.R. 1989. Site-directed mutagenesis by overlap extension using the polymerase chain reaction. *Gene.* 77:51–59.

Kimura, S., Laosinchai, W., Itoh, T., Cui, X., Linder, C. and Brown, R. 1999. Immunogold labeling of rosette terminal cellulose-synthesizing complexes in the vascular plant vigna angularis. *Plant Cell.* 11:2075–2086.

Lei, L., Zhang, T., Strasser, R., Lee, C.M., Gonneau, M., Mach, L., Vernhettes, S., Kim, S.H., Cosgrove, D., Li, S. and Gu, Y. 2014. The *jiaoyao1* mutant is an allele of *korrigan1* that abolishes endoglucanase activity and affects the organization of both cellulose microfibrils and microtubules in Arabidopsis. *Plant Cell.* 26:2601-2616.

Liu, Z., Persson, S., Sanchez-Rodriguez, C. 2015. At the boarder: the plasma membrane-cell wall continuum. *J Exp Bot.* 66:1553-1563.

Miart, F., Desprez, T., Biot, E., Morin, H., Belcram, K., Höfte, H., Gonneau, M. and Vernhettes, S. 2013. Spatio-temporal analysis of cellulose synthesis during cell plate formation in Arabidopsis. *Plant J.* 77:71–84.

Morgan, J.L.W., McNamara, J.T. and Zimmer, J. 2014. Mechanism of activation of bacterial cellulose synthase by cyclic di-GMP. *Nat Struct Mol Biol.* 5:489-496.

Morgan, J.L.W., Strumillo, J. and Zimmer, J. 2013. Crystallographic snapshot of cellulose synthesis and membrane translocation. *Nature.* 493:181–186.

Pauly, M. and Keegstra, K. 2008. Cell-wall carbohydrates and their modification as a resource for biofuels. *Plant J.* 54:559–568.

Peng, L., Hocart, C.H., Redmond, J.W. and Williamson, R.E. 2000. Fractionation of carbohydrates in Arabidopsis root cell walls shows that three radial swelling loci are specifically involved in cellulose production. Planta 211:406–414.

Perroud, P.R. and Quatrano, R.S. 2006. The role of ARPC4 in tip growth and alignment of the polar axis in filaments of Physcomitrella patens. *Cell Motil Cytoskel.* 63:162-171.

Persson, S., Paredez, A., Carroll, A., Palsdottir, H., Doblin, M., Poindexter, P., Khitrov, N., Auer, M. and Somerville, C.R. 2007. Genetic evidence for three unique components in primary cell-wall cellulose synthase complexes in Arabidopsis. *Proc Natl Acad Sci USA.* 104:15566–15571.

Roberts, A.W. and Bushoven, J.T. 2007. The cellulose synthase (CESA) gene superfamily of the moss Physcomitrella patens. *Plant Mol Biol.* 63:207–219.

Roberts, A.W., Roberts, E.M. and Haigler, C.H. 2012. Moss cell walls: structure and biosynthesis. *Front Plant Sci.* 3:1-7.

Scavuzzo-Duggan, T.R., Chaves, A.M and Roberts, A.W. 2015. A complementation assay for in vivo study of protein structure-function relationships in Physcomitrella patens (FUNARIACEAE). *Appl Plant Sci.* doi: http://dx.doi.org/10.3732/apps.1500023

Scheible, W.-R., Eshed, R., Richmond, T., Delmer, D. and Somerville, C. 2001. Modifications of cellulose synthase confer resistance to isoxaben and thiazolidinone herbicides in Arabidopsis Ixr1 mutants. *Proc Natl Acad Sci USA.* 98:10079–10084.

Sethaphong, L., Haigler, C.H., Kubicki, J.D., Zimmer, J., Bonetta, D., DeBolt, S. and Yingling, Y.G. 2013. Tertiary model of a plant cellulose synthase. *Proc Natl Acad Sci USA.* 110:7512–7517.

Slabaugh, E., Davis, J.K., Haigler, C.H., Yingling, Y.G. and Zimmer, J. 2014a. Cellulose synthases: new insights from crystallography and modeling. *Trends Plant Sci.* 2:99-106.

Slabaugh, E., Sethaphong, L., Xiao, C., Amick, J., Anderson, C.T., Haigler, C.H. and Yingling, Y.G. 2014b. Computational and genetic evidence that different structural conformations of a non-catalytic region affect the function of plant cellulose synthase. *J Exp Bot.* 65:6645–6653.

Sokal R.R. and Rohlf F.J. 1981. Biometry. W. H. Freeman and Company, New York

Szymanski, D.B. and Cosgrove, D.J. 2009. Dynamic coordination of cytoskeletal and cell wall systems during plant cell morphogenesis. *Curr Biol.* 19:R800–R811.

Wang, J., Elliott, J.E. and Williamson, R.E. 2008. Features of the primary wall CESA complex in wild type and cellulose-deficient mutants of Arabidopsis thaliana. *J Exp Bot.* 59:2627–2637.

Williamson, R.E., Burn, J.E., Birch, R., Baskin, T.I., Arioli, T., Betzner, A.S. and Cork, A. 2001. Morphology of *rswl*, a cellulose-deficient mutant of Arabidopsis thaliana. *Protoplasma.* 215:116–127.

Zhang, B., Deng, L., Qian, Q., Xiong, G., Zeng, D., Li, R., Guo, L., Li, J. and Zhou, Y. 2009. A missense mutation in the transmembrane domain of CESA4 affects protein abundance in the

plasma membrane and results in abnormal cell wall biosynthesis in rice. *Plant Mol Biol.* 71:509–524.

Zhang, T., Mahgsoudy-Louyeh, S., Tittmann, B. and Cosgrove, D.J. 2014. Visualization of the nanoscale pattern of recently-deposited cellulose microfibrils and matrix materials in never-dried primary walls of the onion epidermis. *Cellulose.* 21:853–862.

Zhang, T., Zheng, Y. and Cosgrove, D.J. 2015. Spatial organization of cellulose microfibrils and matrix polysaccharides in primary plant cell walls as imaged by multi-channel atomic force microscopy. *Plant J. In press*

Zhong, R., Morrison, W.H., Freshour, G.D., Hahn, M.G. and Zheng-Hua, Y. 2003. Expression of a mutant form of cellulose synthase AtCesA7 causes dominant negative effect on cellulose. *Plant Physiol.* 132:786-795.

Figure legends

Fig. 1. The conserved FxVTxK motif occurs between putative TMH5 and TMH6 in plant CESAs (A) Schematic of the predicted topology of CESA with eight putative TMHs indicated by grey boxes. The dashed line indicates the position of the cytosolic domain. (B) Alternate topology of plant CESAs that would be more consistent with the topology of RsBcsA. In this scenario, TMH5 would lie close to the membrane as an interfacial helix (IF). (C) Protein sequence alignment of representative plant and bacterial cellulose synthases showing conservation of the FxVTxK motif in the region designated by the boxes in (A) and (B). See also Supplementary data, Figure S1 and Table S1, for protein sequence identifiers. Arrows and the black line designating the acidic motif indicate residues targeted for mutagenesis in the currently reported research.

Fig. 2. Primary root length and radial swelling phenotypes of *Atcesa1*^{A549V} seedlings expressing mutations to the TMH5-TMH6 region when exposed to a restrictive temperature. Seedlings were grown for five days at a permissive temperature and transferred to a restrictive temperature of 29°C for two additional days. (A) *Atcesa1*^{A549V} seedlings expressing *Atcesa1*^{V956D} or *Atcesa1*^{K959E} retain the short primary root length phenotype, indicating that the amino acid substitutions severely affect AtCESA1 function. *Atcesa1*^{A549V} seedlings expressing either *Atcesa1*^{T952V}, *Atcesa1*$^{mutated\ acidic\ motif}$ or *Atcesa1*$^{deleted\ acidic\ motif}$ all show intermediate primary root lengths compared to Col-0 and the *AtCESA1*$^{wild\ type}$ positive control, indicating that the changes generate partially functional AtCESA1. (B) All mutant lines tested rescued the severe radial swelling that occurs at the root tip of *Atcesa1*^{A549V} seedlings, consistent with incorporation of the mutant

proteins into the CSC at a restrictive temperature. At least three experimental trials were performed, with a total n ≥15 or n ≥30 for measurements of root diameter or length, respectively, in each genotype. Error bars represent standard deviation. Bars with different letters reflect statistically different means (p<0.05, ANOVA). Scale bar equals 0.3 mm.

Fig. 3. Cellulose microfibril anisotropy is lower in the *Atcesa1*^{A549V}, *Atcesa1*^{V956D} and *Atcesa1*^{K959E} roots. Similar to the *Atcesa1*^{A549V} mutant line, the *Atcesa1*^{V956D} and *Atcesa1*^{K959E} mutant lines had low cellulose anisotropy values, indicative of less organized cellulose microfibrils, which is consistent with their persistent short roots. In contrast, no significant differences in anisotropy were observed in the three other mutant lines, wild type, or the *AtCESA1*$^{wild\ type}$ control. Three experimental trials, each with three biological replicates, were performed leading to a total of n ≥39 cells analyzed for anisotropy in each genotype. Error bars represent standard deviation. Bars with different letters reflect statistically different means (p<0.05, ANOVA). Representative micrographs of S4B-stained roots used for analysis with FibrilTool are available in Supplementary data Figure S5.

Fig. 4. Root and hypocotyl lengths of five day old seedlings grown at a lower restrictive temperature of 27°C. (A) Primary root lengths were measured in light-grown seedlings. All mutants tested have shorter primary roots than Col-0 and the positive control (*AtCESA1*$^{wild\ type}$). *Atcesa1*^{V956D} roots were similar in length to *Atcesa1*^{A549V}, however, *Atcesa1*^{K959E} roots were slightly longer than *Atcesa1*^{A549V}. The *Atcesa1*^{T952V}, *Atcesa1*$^{mutated\ acidic\ motif}$ and *Atcesa1*$^{deleted\ acidic\ motif}$ mutants all showed intermediate primary root lengths. (B) Hypocotyl lengths were measured

in dark-grown seedlings. Similarly to the primary root length phenotype, all mutants tested had shorter hypocotyls compared to Col-0 and the positive control (*AtCESA1*$^{wild\ type}$). The *Atcesa1*^{T952V}, *Atcesa1*$^{mutated\ acidic\ motif}$ and *Atcesa1*$^{deleted\ acidic\ motif}$ mutants all showed intermediate hypocotyl lengths. However, the hypocotyls in the *Atcesa1*^{V956D} and *Atcesa1*^{K959E} mutants were more than twice as long than hypocotyls in the *Atcesa1*^{A549V} mutant line. Notably, the lengthening of dark-grown hypocotyls was less hindered by the V956D and K959E mutations as compared to root elongation. At least three experimental replicates were performed for each phenotype, leading to n ≥24 or n ≥42 measurement for root or hypocotyl length, respectively. Error bars represent standard deviation. Bars with different letters reflect statistically different means (p<0.05, ANOVA).

Fig. 5. Atomic force microscopy revealed alterations in hypocotyl inner cell wall architecture of the *Atcesa1*^{A549V} mutant line, but not two experimental mutant lines. All lines were grown for five days at a restrictive temperature of 27°C. (A-D) The *Atcesa1*^{A549V} mutant hypocotyls showed more disordered cell wall architecture compared to the overall parallel orientation observed in Col-0 or the *Atcesa1*^{T952V} and *Atcesa1*^{V956D} mutant hypocotyls, as shown by comparison of these representative images. The areas in the black boxes are displayed at higher magnification in the insets within each panel. (E) Only the *Atcesa1*^{A549V} mutant had cell wall fibrils with wider average diameter when grown at a restrictive temperature (n = 200 measurements from at least four representative images per genotype). Bars with different letters reflect statistically different means (p<0.05, ANOVA). The scale bars in (A) equal 100 nm and apply to the other panels, either the lower magnification images or the insets, as shown in (A).

Fig. 6. The V958D and K961E mutations alter PpCESA5 function. *Ppcesa5* knockout lines expressing *Ppcesa5*^{V958D} and *Ppcesa5*^{K961E} had fewer colonies that produced gametophores compared to the positive control (*PpCESA5*$^{wild\ type}$), but more colonies that produced gametophores than the negative control (empty vector). In contrast, the *Ppcesa5*^{T954V}, *Ppcesa5*$^{mutated\ acidic\ motif}$ and *Ppcesa5*$^{deleted\ acidic\ motif}$ mutations all resulted in a similar number of colonies that produced gametophores compared to wild type. Bars with different letters reflect statistically different means within each set of histograms (p<0.05, Fisher's exact test).

Table 1. Summarized phenotypic data and nature of mutations for AtCESA1 and PpCESA5

AtCESA1 mutation	Rescue root length?[1]	Rescue root swelling?[1]	PpCESA5 mutation	Rescue gameto-phores?[2]	Amino acid change
T952V	Partial	Yes	T954V	Yes	Polar uncharged to hydrophobic
F954L (Slabaugh *et al*. 2014b)	No	ND	F956L	Partial	Aromatic to hydrophobic
V956D	No	Yes	V958D	Partial	Hydrophobic to acidic
K959E	No	Yes	K961E	Partial	Basic to acidic
mutated acidic motif (DEDGD to NQNGN)	Partial	Yes	mutated acidic motif (DDED to NNQN)	Yes	Removal of acidic charge
deleted acidic motif (DEDGD)	Partial	Yes	deleted acidic motif (DDED)	Yes	Deletion of 4-5 amino acids

[1]In AtCESA1 experiments, phenotypes arising from the background *rsw1-1* mutation were short roots and swollen root tips at restrictive temperature.

[2]In PpCESA5 experiments, the knock-out line had fewer colonies with gametophores as compared to wild type.

ND: Not determined.

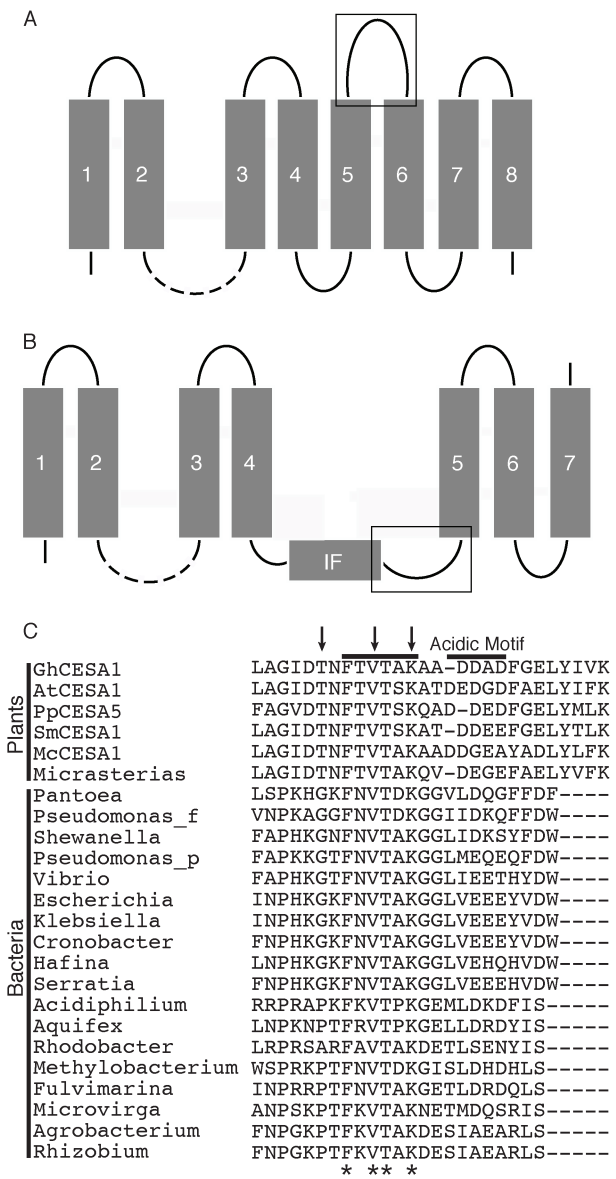

Fig. 1. The conserved FxVTxK motif occurs between putative TMH5 and TMH6 in plant CESAs (A) Schematic of the predicted topology of CESA with eight putative TMHs indicated by grey boxes. The dashed line indicates the position of the cytosolic domain. (B) Alternate topology of plant CESAs that would be more consistent with the topology of RsBcsA. In this scenario, TMH5 would lie close to the membrane as an interfacial helix (IF). (C) Protein sequence alignment of representative plant and bacterial cellulose synthases showing conservation of the FxVTxK motif in the region designated by the boxes in (A) and (B). See also Supplementary data, Figure S1 and Table S1, for protein

sequence identifiers. Arrows and the black line designating the acidic motif indicate residues targeted for mutagenesis in the currently reported research.

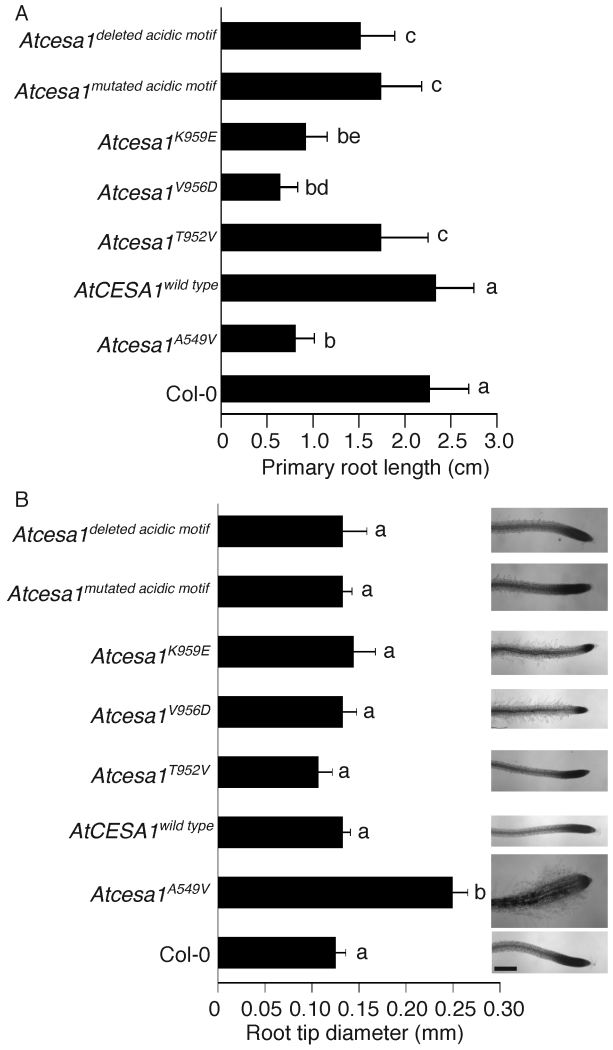

Fig. 2. Primary root length and radial swelling phenotypes of *Atcesa1*^{A549V} seedlings expressing mutations to the TMH5-TMH6 region when exposed to a restrictive temperature. Seedlings were grown for five days at a permissive temperature and transferred to a restrictive temperature of 29°C for two additional days. (A) *Atcesa1*^{A549V} seedlings expressing *Atcesa1*^{V956D} or *Atcesa1*^{K959E} retain the short primary root length phenotype, indicating that the amino acid substitutions severely affect AtCESA1 function. *Atcesa1*^{A549V} seedlings expressing either *Atcesa1*^{T952V}, *Atcesa1*$^{mutated\ acidic\ motif}$ or *Atcesa1*$^{deleted\ acidic\ motif}$ all show intermediate primary root lengths compared to Col-0 and the *AtCESA1*$^{wild\ type}$ positive control, indicating that the changes generate partially functional AtCESA1. (B) All mutant lines tested rescued the severe radial swelling that occurs at the root tip of *Atcesa1*^{A549V} seedlings, consistent with incorporation of the mutant proteins into the CSC at a restrictive temperature. At least three experimental

trials were performed, with a total n ≥15 or n ≥30 for measurements of root diameter or length, respectively, in each genotype. Error bars represent standard deviation. Bars with different letters reflect statistically different means (p<0.05, ANOVA). Scale bar equals 0.3 mm.

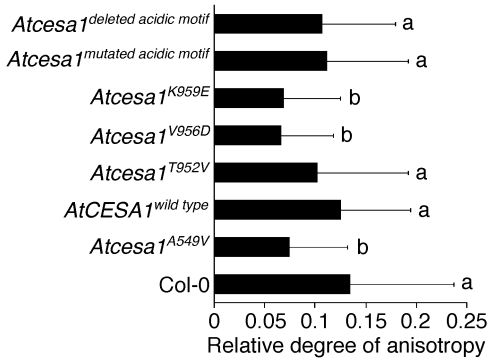

Fig. 3. Cellulose microfibril anisotropy is lower in the *Atcesa1*^{A549V}, *Atcesa1*^{V956D} and *Atcesa1*^{K959E} roots. Similar to the *Atcesa1*^{A549V} mutant line, the *Atcesa1*^{V956D} and *Atcesa1*^{K959E} mutant lines had low cellulose anisotropy values, indicative of less organized cellulose microfibrils, which is consistent with their persistent short roots. In contrast, no significant differences in anisotropy were observed in the three other mutant lines, wild type, or the *AtCESA1*$^{wild\ type}$ control. Three experimental trials, each with three biological replicates, were performed leading to a total of n ≥39 cells analyzed for anisotropy in each genotype. Error bars represent standard deviation. Bars with different letters reflect statistically different means (p<0.05, ANOVA). Representative micrographs of S4B-stained roots used for analysis with FibrilTool are available in Supplementary data Figure S5.

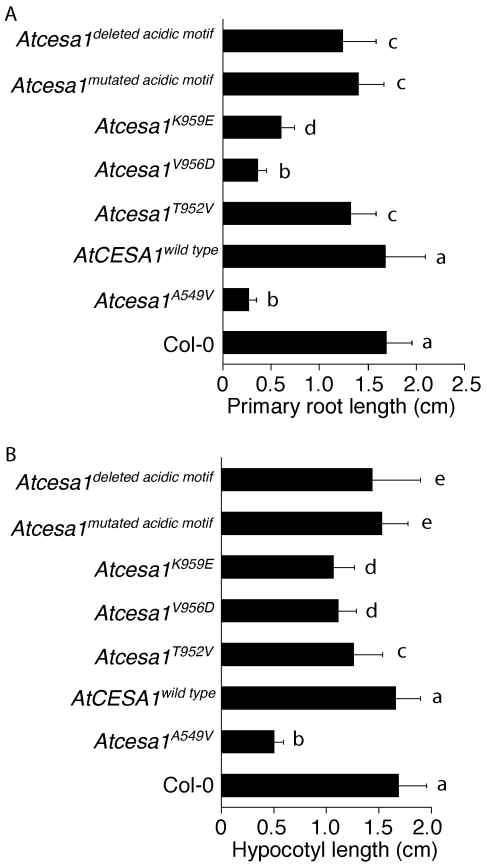

Fig. 4. Root and hypocotyl lengths of five day old seedlings grown at a lower restrictive temperature of 27°C. (A) Primary root lengths were measured in light-grown seedlings. All mutants tested have shorter primary roots than Col-0 and the positive control (*AtCESA1*$^{wild\ type}$). *Atcesa1*^{V956D} roots were similar in length to *Atcesa1*^{A549V}, however, *Atcesa1*^{K959E} roots were slightly longer than *Atcesa1*^{A549V}. The *Atcesa1*^{T952V}, *Atcesa1*$^{mutated\ acidic\ motif}$ and *Atcesa1*$^{deleted\ acidic\ motif}$ mutants all showed intermediate primary root lengths. (B) Hypocotyl lengths were measured in dark-grown seedlings. Similarly to the primary root length phenotype, all mutants tested had shorter hypocotyls compared to Col-0 and the positive control (*AtCESA1*$^{wild\ type}$). The *Atcesa1*^{T952V}, *Atcesa1*$^{mutated\ acidic\ motif}$ and *Atcesa1*$^{deleted\ acidic\ motif}$ mutants all showed intermediate hypocotyl lengths. However, the hypocotyls in the *Atcesa1*^{V956D} and *Atcesa1*^{K959E} mutants were more than twice as long than hypocotyls in the *Atcesa1*^{A549V} mutant line. Notably, the lengthening of dark-grown hypocotyls was less hindered by the V956D and K959E mutations as compared to root elongation. At least three experimental replicates were performed for each phenotype, leading to n ≥24 or n ≥42 measurement for root or hypocotyl length, respectively. Error bars represent standard deviation. Bars with different letters reflect statistically different means (p<0.05, ANOVA).

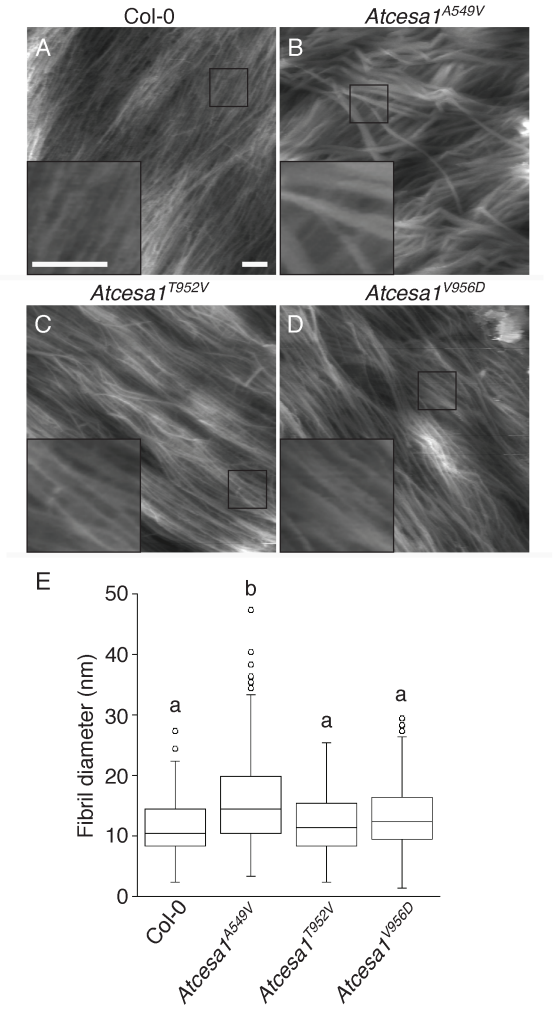

Fig. 5. Atomic force microscopy revealed alterations in hypocotyl inner cell wall architecture of the *Atcesa1*^{A549V} mutant line, but not two experimental mutant lines. All lines were grown for five days at a restrictive temperature of 27°C. (A-D) The *Atcesa1*^{A549V} mutant hypocotyls showed more disordered cell wall architecture compared to the overall parallel orientation observed in Col-0 or the *Atcesa1*^{T952V} and *Atcesa1*^{V956D} mutant hypocotyls, as shown by comparison of these representative images. The areas in the black boxes are displayed at higher magnification in the insets within each panel. (E) Only the *Atcesa1*^{A549V} mutant had cell wall fibrils with wider average diameter when grown at a restrictive temperature (n = 200 measurements from at least four representative images per genotype). Bars with different letters reflect statistically different means (p<0.05, ANOVA). The scale bars in (A) equal 100 nm and apply to the other panels, either the lower magnification images or the insets, as shown in (A).

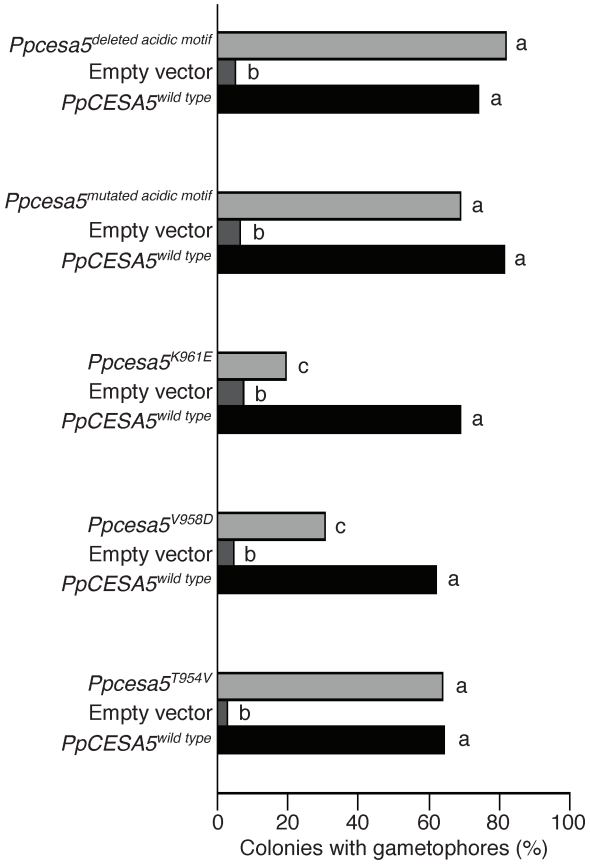

Fig. 6. The V958D and K961E mutations alter PpCESA5 function. *Ppcesa5* knockout lines expressing *Ppcesa5*^{V958D} and *Ppcesa5*^{K961E} had fewer colonies that produced gametophores compared to the positive control (*PpCESA5*$^{wild\ type}$), but more colonies that produced gametophores than the negative control (empty vector). In contrast, the *Ppcesa5*^{T954V}, *Ppcesa5*$^{mutated\ acidic\ motif}$ and *Ppcesa5*$^{deleted\ acidic\ motif}$ mutations all resulted in a similar number of colonies that produced gametophores compared to wild type. Bars with different letters reflect statistically different means within each set of histograms (p<0.05, Fisher's exact test).

The valine and lysine residues in the conserved FxVTxK motif are important for the function of phylogenetically distant plant cellulose synthases

Erin Slabaugh, Tess Scavuzzo-Duggan, Arielle Chaves, Liza Wilson, Carmen Wilson, Jonathan K. Davis, Daniel J. Cosgrove, Charles T. Anderson, Alison W. Roberts and Candace H. Haigler

Supplementary Figures

Fig. S1. Conservation of the FxVTxK motif in plant and bacterial cellulose synthase protein sequences. Analysis of the FxVTxK motif from 73 plant and 25 bacterial cellulose synthase sequences revealed the high conservation of the F, V, T and K residues in this motif. Logo motif generation was performed using WebLogo (Crooks et al. 2004). GenBank IDs of protein sequences can be found in Table S1.

(Figures S2 – S7 and Supplementary References are available on the following pages. Supplementary Tables are in a different file.)

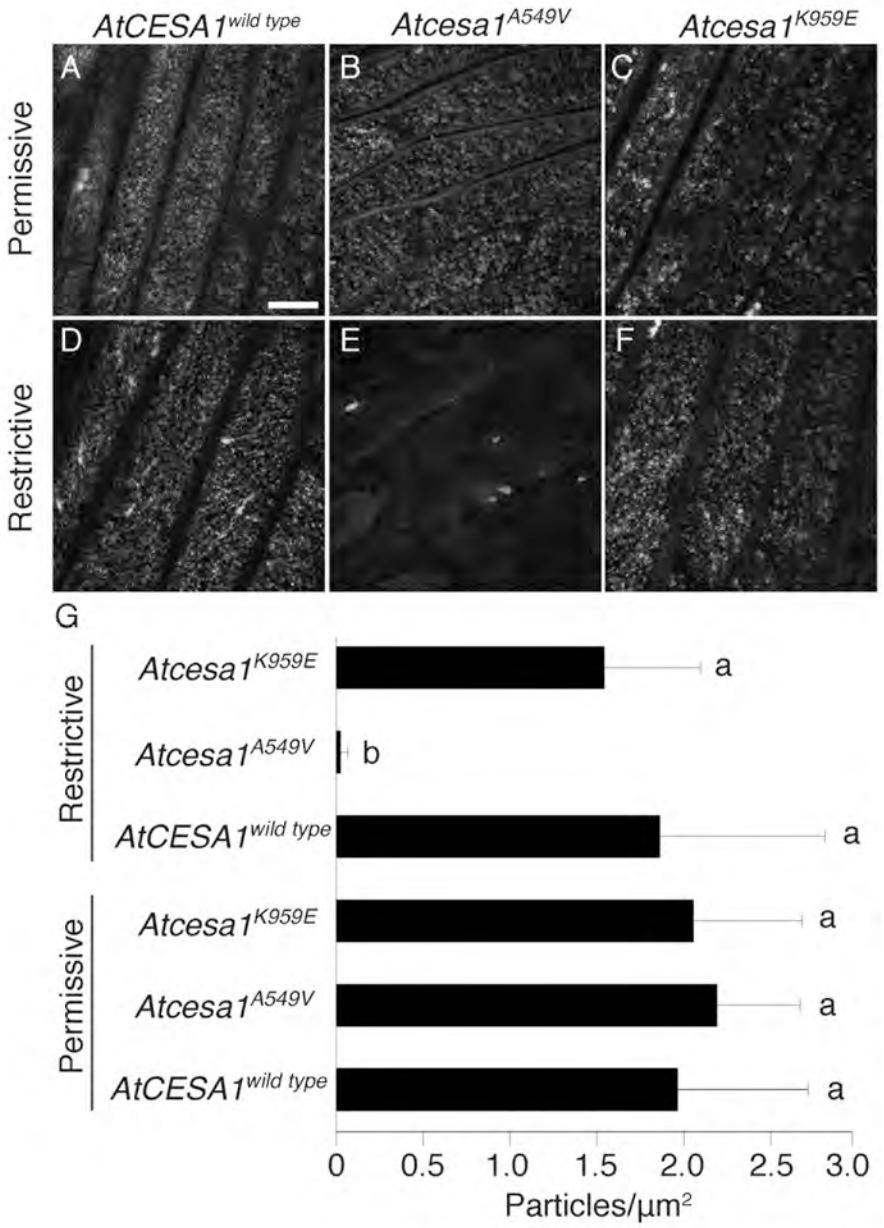

Fig. S2. Subcellular localization of YFP-CESA6 near the plasma membrane at a restrictive temperature confirms protein expression of AtCESA1^{K959E}. Stable transformants expressing *Atcesa1*^{K959E} in the *Atcesa1*^{A549V} YFP-CESA6 background were used to indirectly monitor AtCESA1^{K959E} protein expression. Hypocotyls were either grown for three days at a permissive temperature (22°C) or two days at a permissive temperature and one day at a restrictive temperature (29°C). (A-F) Representative images from laser scanning confocal microscopy of the plasma membrane region. (A-C) YFP-CESA6 was visualized as fluorescent punctae near the plasma membrane in hypocotyls grown at a permissive temperature in all three lines, as expected. (E) Lack of fluorescence near the plasma membrane was consistent with the redistribution of YFP-CESA6 to endomembrane compartments in *Atcesa1*^{A549V} YFP-CESA6 hypocotyls when

grown at a restrictive temperature. (D and F) In contrast, seedlings also expressing the wild type or K959E allele of AtCESA1 maintained YFP-CESA6 near the plasma membrane as indicated by fluorescent puncta. (G) Quantification of particle density in the plasma membrane region showed that YFP-CESA6 persisted at the plasma membrane at 29°C when AtCESA1^{K959E} was used to complement the *Atcesa1*^{A549V} mutation. These results provide an explanation for the rescue of the radial swelling phenotype and support protein expression of AtCESA1^{K959E} and the formation of the CSC. Microscopic analysis was as described in Materials and Methods for *Laser scanning confocal microscopy*. Particle density was measured in at least eleven individual cells from at least three individual hypocotyls. Error bars represent standard deviation. Bars with different letters reflect statistically different means (p<0.05, ANOVA). Scale bar equals 10 μm.

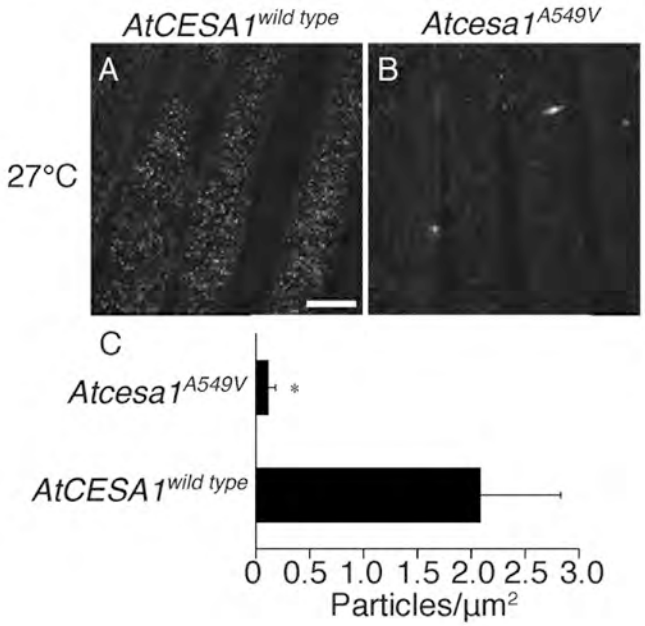

Fig. S3. Depletion of YFP-CESA6 near the plasma membrane confirms temperature sensitivity of the *Atcesa1*^{A549V} allele at a lower restrictive temperature of 27°C. *Atcesa1*^{A549V} YFP-CESA6 hypocotyls and *Atcesa1*^{A549V} YFP-CESA6 hypocotyls expressing *AtCESA1*$^{wild\ type}$ were grown for two days at 22°C and then transferred to 27°C for one day. (A) YFP-CESA6 was visualized as fluorescent puncta near the plasma membrane in hypocotyls expressing *AtCESA1*$^{wild\ type}$. (B) In contrast, YFP-CESA6 was greatly depleted from the plasma membrane in *Atcesa1*^{A549V} YFP-CESA6 hypocotyls. (C) Particle density in the plasma membrane region was calculated in replicates for both lines, confirming visual evidence. These data indicate that the *Atcesa1*^{A549V} allele does not support the existence of CSCs near the plasma membrane. Microscopic analysis was as described in Materials and Methods for *Laser scanning confocal microscopy.* Particle density was measured in at least seventeen individual cells from at least five individual hypocotyls. Error bars represent standard deviation. Asterisk indicates a significant difference compared to the control (p<0.05, Student's t-test). Scale bar equals 10 μm.

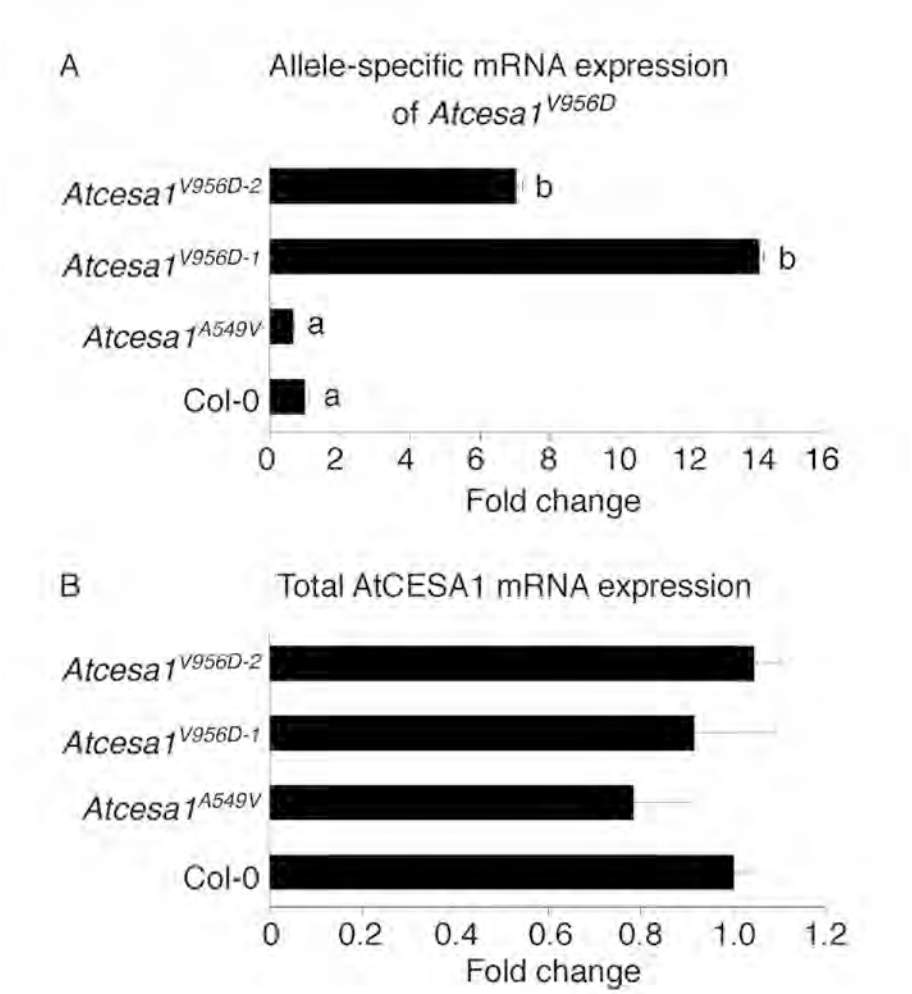

Fig. S4. Allele-specific qRT-PCR showed that *Atcesa1*^{V956D} mRNA was expressed in the *Atcesa1*^{V956D} line. (A) The *Atcesa1*^{V956D} transcript was expressed 7 to 14 fold higher in two independent *Atcesa1*^{V956D} lines compared to Col-0. (B) Total AtCESA1 mRNA expression showed no significant difference across all four lines tested. All seedlings were grown for five days at a permissive temperature (22°C) and transferred to a restrictive temperature (29°C) for two additional days. Fold change was measured relative to Col-0 in (A) and (B). Error bars represent standard deviation. Bars with different letters reflect statistically different means (p<0.05, ANOVA).

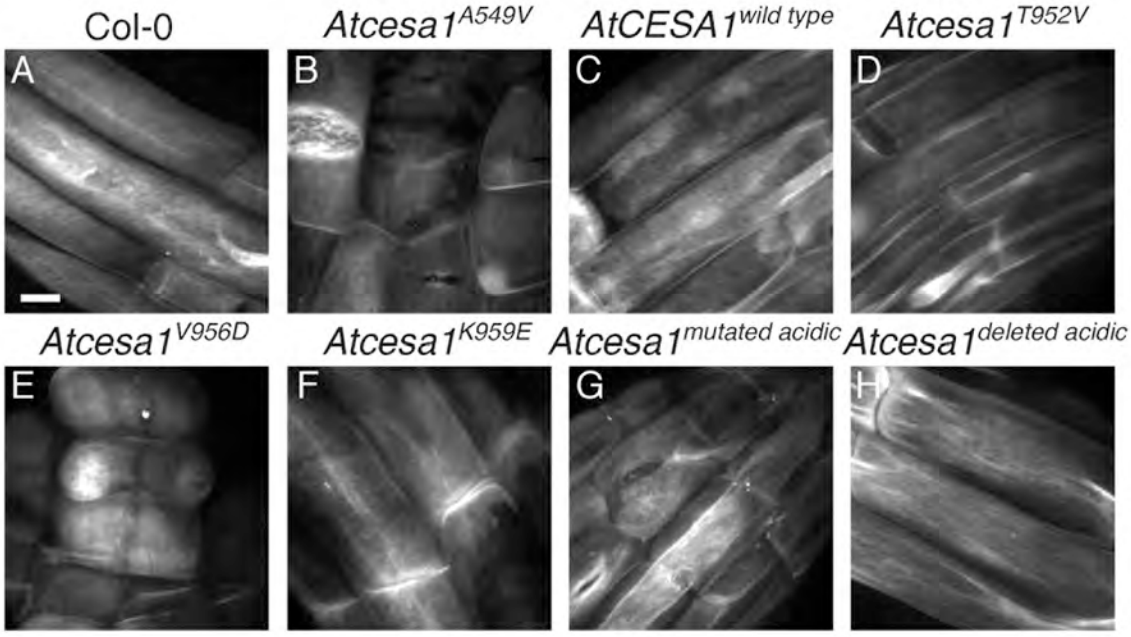

Fig. S5. Visualization of S4B-stained cellulose microfibrils by confocal microscopy. Seedlings were grown for 5 days at a restrictive temperature (27°C). Col-0 is the wild type line, *Atcesa1*^{A549V} is the uncomplemented mutant line, and *AtCESA1*$^{wild\ type}$ is the *Atcesa1*^{A549V} line rescued with native *AtCESA1*. All other panels represent the indicated mutant gene expressed in the *Atcesa1*^{A549V} background line. Nine seedlings per genotype were analyzed within three independent experimental trials. Scale bar equals 10 μm.

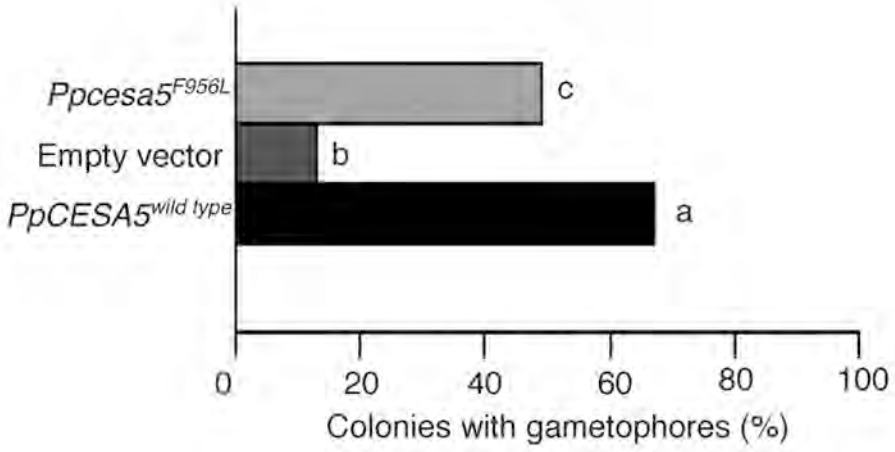

Fig. S6. Mutation of the conserved phenylalanine residue in the FxVTxK motif affects PpCESA5 function. This line was generated to parallel results previously published for Arabidopsis (Slabaugh *et al.* 2014). Expression of the *Ppcesa5*^{F956L} allele in the *Ppcesa5* knock-out line partially complemented the deficit in gametophore formation (empty vector negative control) as compared to the positive control (*PpCESA5*$^{wild\ type}$). Bars with different letters reflect statistically different means (p<0.05, Fisher's exact test).

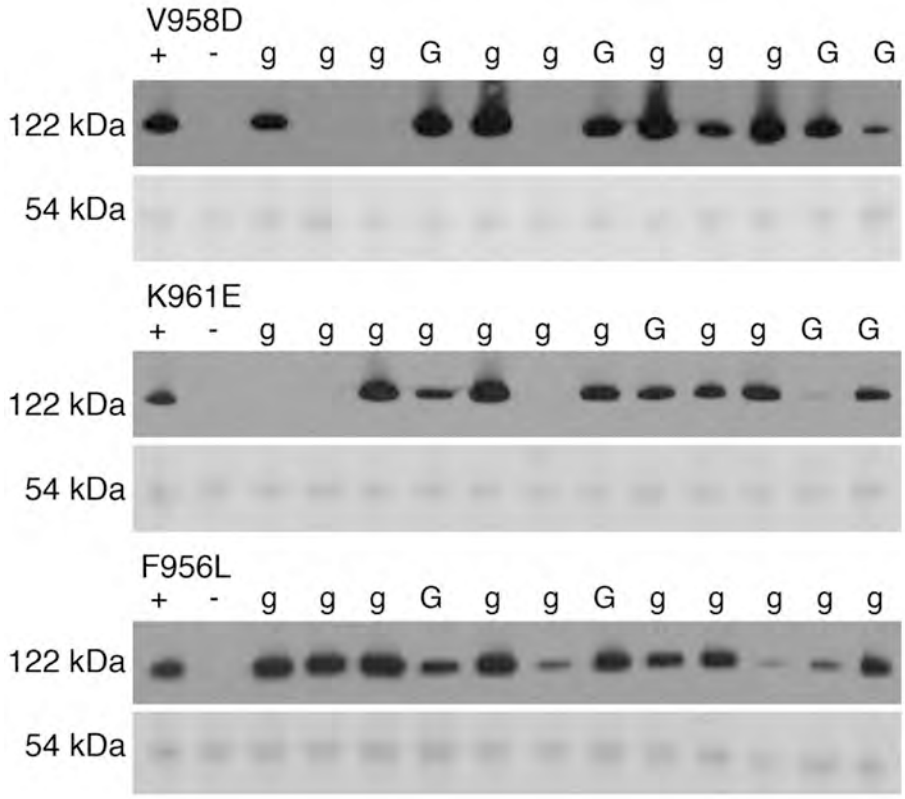

Fig. S7. Western blot analysis of microsomal proteins showed that a mutant PpCESA5 protein was expressed in Physcomitrella transgenic lines lacking complete rescue of gametophore formation (*Ppcesa5*^{F956L}, *Ppcesa5*^{V958D} and *Ppcesa5*^{K961E}). The protein in each lane was extracted from a different colony with (G) or without (g) normal gametophores. The results for the positive control complemented with wild type PpCESA5 or the empty vector negative control are indicated by '+' or '-', respectively. PpCESA5 had an expected molecular weight of 122 kDa (kilo Daltons). Ponceau staining of the 54 kDa region was used as an indicator of similar protein loading. Many of the 'g' lines that lacked gametophores contained the altered PpCESA5 protein, indicating that CESA function was altered by the experimental amino acid substitution. Additional details about this protein expression assay are available in Scavuzzo-Duggan *et al.* 2015.

Supplemental References

Crooks, G.E., Hon, G., Chandonia, J.-M. and Brenner, S.E. (2004) WebLogo: A sequence logo generator. Genome Res 14:1188-1190.

Scavuzzo-Duggan, T.R., Chaves, A.M and Roberts, A.W. (2015) A complementation assay for in vivo study of protein structure-function relationships in Physcomitrella patens (FUNARIACEAE). Appl Plant Sci doi: http://dx.doi.org/10.3732/apps.1500023

Slabaugh, E., Sethaphong, L., Xiao, C., Amick, J., Anderson, C.T., Haigler, C.H. and Yingling, Y.G. (2014) Computational and genetic evidence that different structural conformations of a non-catalytic region affect the function of plant cellulose synthase. J Exp Bot 65:6645–6653.

The valine and lysine residues in the conserved FxVTxK motif are important for the function of phylogenetically distant plant cellulose synthases

Erin Slabaugh, Tess Scavuzzo-Duggan, Arielle Chaves, Liza Wilson, Carmen Wilson, Jonathan K. Davis, Daniel J. Cosgrove, Charles T. Anderson, Alison W. Roberts and Candace H. Haigler

Table S1. Gene, species, motif sequence and GenBankID numbers for generation of the FxVTxK logo motif in Figure S1.

Plants			Bacteria		
Gene	**Sequence**	**GenBank ID**	**Species**	**Sequence**	**GenBankID**
AtCESA1	FTVTSK	NP_194967	*Acaryochloris marina*	FQVTPK	WP_012165112.1
AtCESA10	FTVTSK	AHL38838.1	*Acidiphilium cryptum*	FKVTPK	WP_011941613.1
AtCESA2	FTVTSK	NP_195645.1	*Agrobacterium tumefaciens*	FKVTAK	AAC41436.1
AtCESA3	FTVTSK	AAC39336.1	*Aquifex aeolicus*	FRVTPK	WP_010880909.1
AtCESA4	FTVTSK	NP_199216.2	*Coleofasciculus chthonoplastes*	FQVTPK	WP_006102136.1
AtCESA5	FTVTSK	NP_196549.1	*Cronobacter sakazakii*	FNVTAK	WP_007871858.1
AtCESA6	FTVTSK	NP_201279.1	*Cyanobacterium stanieri*	FKVTPK	WP_015222622.1
AtCESA7	FTVTSK	AAD32031.1	*Escherichia coli*	FNVTAK	WP_023142525.1
AtCESA8	FTVTSK	NP_567564.1	*Fulvimarina pelagi*	FNVTAK	WP_007066049.1
AtCESA9	FTVTSK	NP_179768.1	*Hafnia alvei*	FNVTAK	EHM44710.1
GhCESA1	FTVTAK	AAB37766.1	*Klebsiella pneumoniae*	FNVTAK	EJK89443.1
GhCESA2	FTVTSK	AAN28291.1	*Leptolyngbya_PCC7375*	FKVTPK	WP_006519065.1
GhCESA3	FTVTSK	AAD39534.2	*Leptolyngbya_PCC7376*	FKVTPK	WP_015135547.1
GhCESA4	FTVTAK	AAL37718.1	*Methylobacterium extorquens*	FNVTDK	WP_015822009.1
GhCESA5	FTVTSK	AFB18634.1	*Microvirga flocculans*	FKVTAK	WP_027314669.1
GhCESA7	FTVTSK	KHG11460.1	*Pantoea vagans*	FNVTDK	ADO11491.1
GhCESA8	FTVTAK	ABG06122.1	*Pleurocapsa sp. PCC 7319*	FQVTPK	WP_019505068.1
GhCESA9	FTVTSK	ACS88358.1	*Pseudomonas fluorescens*	FNVTDK	WP_012721722.1
McCESA1	FTVTAK	AAM83096.1	*Pseudomonas putida*	FNVTAK	WP_010953555.1
McCESA2	FTVTAK	AAT48369.1	*Rhizobium lupini*	FKVTAK	WP_006698566.1
Micrasterias denticulata	FTVTAK	ADE44904.1	*Rhodobacter sphaeroides*	FAVTAK	YP_353410.1
OsCESA1	FTVTSK	NP_001054788.1	*Serratia proteamaculans*	FNVTAK	WP_012004620.1
OsCESA2	FTVTSK	NP_001051648.1	*Shewanella violacea*	FNVTAK	WP_013049415.1
OsCESA3	FTVTSK	NP_001059487.1	*Synechococcus sp. PCC 7002*	FEVTPK	WP_012307721.1
OsCESA4	FTVTAK	NP_001044252.1	*Vibrio fischeri*	FNVTAK	WP_011263701.1
OsCESA5	FTVTSK	NP_001051830.1			
OsCESA6	FTVTSK	NP_001059303.1			
OsCESA7	FTVTSK	NP_001064811.1			

OsCESA8	FTVTSK	NP_001059162.1
Penium margaritaceum	FTVTAK	HO618573.1
PpCESA10	FTVTSK	XP_001776974.1
PpCESA3	FTVTSK	XP_001753310.1
PpCESA4	FTVTSK	XP_001767133.1
PpCESA5	FTVTSK	ABI78958.1
PpCESA6	FTVTSK	ABI78959.1
PpCESA7	FTVTSK	ABI78960.1
PpCESA8	FTVTSK	XP_001769255.1
PpCESA9	FTVTSK	DQ902550
PtaCESA1	FTVTAK	AAX18647.1
PtaCESA2	FTVTAK	AAX18648.1
PtaCESA3	FTVTAK	AAX18649.1
PtCESA1	FTVTSK	XP_002308657.1
PtCESA10	FTVTSK	XP_002324291.1
PtCESA11	FTVTSK	EEE92180.1
PtCESA12	FTVTSK	XP_002308955.1
PtCESA13	FTVTSK	XP_002314037.1
PtCESA14	FTVTSK	XP_002322712.1
PtCESA15	FTVTSK	XP_002319002.2
PtCESA16	FTVTSK	XP_006382504.1
PtCESA17	FTVTSK	XP_002325122.1
PtCESA18	FTVTAK	XP_002305060.1
PtCESA2	FTVTSK	XP_002302169.1
PtCESA3	FTVTSK	XP_006369625.1
PtCESA4	FTVTSK	AGW52051.1
PtCESA5	FTVTSK	XP_002306707.1
PtCESA6	FTVTSK	XP_002307145.1
PtCESA7	FTVTSK	XP_002308412.1
PtCESA8	FTVTAK	XP_002316815.1
PtCESA9	FTVTSK	XP_002310628.1
SmCESA1	FTVTSK	XP_002963550.1
SmCESA2	FTVTSK	XP_002960719.1
SmCESA3	FTVTTK	XP_002960291.1
SmCESA4	FTVTSK	XP_002960761
ZmCESA1	FTVTSK	NP_001104954.1
ZmCESA10	FTVTSK	NP_001105672.1
ZmCESA11	FTVTAK	NP_001105236.1
ZmCESA12	FTVTSK	NP_001105532.1
ZmCESA2	FTVTSK	NP_001105574.1

ZmCESA4	FTVTSK	NP_001105621.1
ZmCESA5	FTVTSK	NP_001104955.1
ZmCESA6	FTVTSK	NP_001104956
ZmCESA7	FTVTSK	NP_001104957.1
ZmCESA8	FTVTSK	NP_001104958.1
ZmCESA9	FTVTSK	NP_001104959.1

Table S2. Primary root length of all independent lines analyzed when grown for 5 d at 22°C and 2 d at 29°C. The average root length, standard deviations and n values are listed for all mutant lines phenotyped. All mutants were tested in both the *Atcesa1*^{A549V} (rsw1) and *Atcesa6*^{prc1} *Atcesa1*^{A549V} YFP-CESA6 (p/r Y-6) backgrounds, except *Atcesa1*$^{mutated\ acidic\ motif}$ that was only analyzed in p/r Y-6. Overall, there was little variation in the extent of phenotypic rescue between independent lines expressing the same mutation. Col-0 represents wild type. Other lines reflect rescues with wild-type AtCESA1 (CESA1 wt) or AtCESA1 with the amino acid or motif change as indicated, with -1 and -2 indicating independent lines for the same genotype.

Genotype	**Avg (cm)**	**Std. dev.**	**n**
Col-0	2.33	0.45	65
rsw1	0.78	0.21	67
p/r Y-6	0.65	0.21	20
rsw1 CESA1 wt	2.39	0.45	51
p/r Y-6 CESA1 wt	2.21	0.39	28
rsw1 T952V-1	1.83	0.47	35
rsw1 T952V-2	1.87	0.52	42
p/r Y-6 T952V-1	1.75	0.57	9
p/r Y-6 T952V-2	1.55	0.42	8
rsw1 V956D-1	0.64	0.20	84
rsw1 V956D-2	0.71	0.17	21
p/r Y-6 V956D-1	0.91	0.21	9
p/r Y-6 V956D-2	0.92	0.21	5
rsw1 K959E-1	0.96	0.26	23
rsw1 K959E-2	0.82	0.24	44
p/r Y-6 K959E-1	0.84	0.21	4
p/r Y-6 K959E-2	0.63	0.17	28
p/r Y-6 acidic motif mutated-1	1.86	0.45	30
p/r Y-6 acidic motif mutated-2	1.70	0.45	52
rsw1 deleted acidic motif-1	1.64	0.43	16
rsw1 deleted acidic motif-2	1.57	0.55	39
p/r Y-6 deleted acidic motif-1	1.56	0.54	6
p/r Y-6 deleted acidic motif-2	1.46	0.60	5

Table S3. Primer sequences used for mutagenesis in AtCESA1 and PpCESA5 and qPCR analysis of AtCESA1.

Mutagenesis	**F/R**	**5' to 3'**
Atcesa1^{T952V}	F	GGTATCGACGTCAACTTCACCG
	R	CGGTGAAGTTGACGTCGATACC
Atcesa1^{V956D}	F	GACACCAACTTCACCGATACATCTAAAGCC
	R	GGCTTTAGATGTATCGGTGAAGTTGGTGTC
Atcesa1^{K959E}	F	CCGTTACATCTGAAGCCACAGACG
	R	CGTCTGTGGCTTCAGATGTAACGG
Atcesa1$^{mutated\ acidic\ motif}$	F	CTAAAGCCACAAACCAAAATGGGAATTTTGCAGAACTC
	R	GAGTTCTGCAAAATTCCCATTTTGGTTTGTGGCTTTAG
Atcesa1$^{deleted\ acidic\ motif}$	F	CCGTTACATCTAAAGCCACATTTGCAGAACTCTACATC
	R	GATGTAGAGTTCTGCAAATGTGGCTTTAGATGTAACGG
Ppcesa5^{T954V}	F	GCCGGAGTGGACGTGAATTTCACCGTC
	R	GACGGTGAAATTCACGTCCACTCCGGC
Ppcesa5^{V958D}	F	ACGAATTTCACCGACACTTCCAAACAA
	R	TTGTTTGGAAGTGTCGGTGAAATTCGT
Ppcesa5^{K961E}	F	ACCGTCACTTCCGAACAAGCAGACGAC
	R	GTCGTCTGCTTGTTCGGAAGTGACGGT
Ppcesa5$^{mutated\ acidic\ motif}$	F	TCCAAACAAGCAAACAACCAAAATTTCGGGGAGCTG
	R	CAGCTCCCCGAAATTTTGGTTGTTTGCTTGTTTGGA
Ppcesa5$^{\text{deleted acidic motif}}$	F	ACTTCCAAACAAGCATTCGGGGAGCTGTACAT
	R	ATGTACAGCTCCCCGAATGCTTGTTTGGAAGT
qPCR		
AtCESA1 universal	F	TAAACAGTGGCTACCAGTCGTGGG
AtCESA1 universal	R	GGTTGGTGTTCGGTTTTGTCTTCCC
AtCESA1 V956 (wild type)	F	CTGGTATCGACACCAACTTCACCGT
AtCESA1 D956 (mutant)	F	CTGGTATCGACACCAACTTCACCGA
AtCESA1 reverse primer for both V956 and D956	R	CATAAGAGACACCAGCCACAATGCC
UBQ10	F	GGCCTTGTATAATCCCTGATGAATAAG
UBQ10	R	AAAGAGATAACAGGAACGGAAACATAGT